Seasonal and event dynamics of spatial soil moisture patterns at the small catchment scale

U. Rosenbaum,[1] H. R. Bogena,[1] M. Herbst,[1] J. A. Huisman,[1] T. J. Peterson,[2] A. Weuthen,[1] A. W. Western,[2] and H. Vereecken[1]

Received 15 October 2011; revised 5 July 2012; accepted 31 August 2012; published 27 October 2012.

[1] Our understanding of short- and long-term dynamics of spatial soil moisture patterns is limited due to measurement constraints. Using new highly detailed data, this research aims to examine seasonal and event-scale spatial soil moisture dynamics in the topsoil and subsoil of the small spruce-covered Wüstebach catchment, Germany. To accomplish this, univariate and geo-statistical analyses were performed for a 1 year long 4-D data set obtained with the wireless sensor network SoilNet. We found large variations in spatial soil moisture patterns in the topsoil, mostly related to meteorological forcing. In the subsoil, temporal dynamics were diminished due to soil water redistribution processes and root water uptake. Topsoil range generally increased with decreasing soil moisture. The relationship between the spatial standard deviation of the topsoil soil moisture (SD_θ) and mean water content ($\overline{\theta}$) showed a convex shape, as has often been found in humid temperate climate conditions. Observed scatter in topsoil $SD_\theta(\overline{\theta})$ was explained by seasonal and event-scale $SD_\theta(\overline{\theta})$ dynamics, possibly involving hysteresis at both time scales. Clockwise hysteretic $SD_\theta(\overline{\theta})$ dynamics at the event scale were generated under moderate soil moisture conditions only for intense precipitation that rapidly wetted the topsoil and increased soil moisture variability controlled by spruce throughfall patterns. This hysteretic effect increased with increasing precipitation, reduced root water uptake, and high groundwater level. Intense precipitation on dry topsoil abruptly increased SD_θ but only marginally increased mean soil moisture. This was due to different soil rewetting behavior in drier upslope areas (hydrophobicity and preferential flow caused minor topsoil recharge) compared with the moderately wet valley bottom (topsoil water storage), which led to a more spatially organized pattern. This study showed that spatial soil moisture patterns monitored by a wireless sensor network varied with depth, soil moisture content, seasonally, and within single wetting and drying episodes. This was controlled by multiple factors including soil properties, topography, meteorological forcing, vegetation, and groundwater.

Citation: Rosenbaum, U., H. R. Bogena, M. Herbst, J. A. Huisman, T. J. Peterson, A. Weuthen, A. W. Western, and H. Vereecken (2012), Seasonal and event dynamics of spatial soil moisture patterns at the small catchment scale, *Water Resour. Res.*, *48*, W10544, doi:10.1029/2011WR011518.

1. Introduction

[2] Soil moisture θ varies strongly in space and time and is controlled by complex interacting environmental factors (e.g., soil properties, topography, radiation, precipitation, vegetation) that also change in space and time. Soil moisture is known to affect important processes including evapotranspiration and runoff in a nonlinear manner [*Western et al.*, 2002]. It is widely recognized that improved understanding of the dynamics of spatial soil moisture patterns can yield valuable insights into hydrological processes [*Grayson et al.*, 1997; *Grayson and Blöschl*, 2000; *Robinson et al.*, 2008, *Vereecken et al.*, 2008; *Blume et al.*, 2009; *Zehe et al.*, 2010].

[3] Catchment-scale soil moisture measurement campaigns often support remote sensing surveys and thus typically provide area-wide but near-surface (<5 cm) soil moisture information for agricultural and pasture fields at selected points in time [*Walker et al.*, 2004]. A few studies (e.g., in the Tarrawarra experimental test site) have mapped soil moisture with mobile time domain reflectometry instruments [e.g., *Western and Grayson*, 1998]. Other monitoring campaigns led to area-wide measurements at multiple depths in small forested catchments (e.g., Shale Hills Critical Zone Observatory) for several years with temporal resolution ranging from daily to weekly measurements [e.g., *Lin*, 2006; *Takagi and Lin*, 2011]. In contrast, permanent measurements (e.g., with capacitance sensors or time domain reflectometry)

[1]Agrosphere Institute, IBG-3, Forschungszentrum Jülich GmbH, Jülich, Germany.
[2]Department of Infrastructure Engineering, University of Melbourne, Victoria, Australia.

Corresponding author: U. Rosenbaum, Agrosphere Institute, IBG-3, Forschungszentrum Jülich GmbH, 52425 Jülich, Germany. (ulrike.rosenbaum@tu-berlin.de)

0043-1397/12/2011WR011518

typically provide long-term data for several depths at a few locations with a high temporal resolution [e.g., *Graham and Lin*, 2011]. Thus, soil moisture data at the catchment scale are often available at either a high spatial or high temporal resolution [e.g., *De Lannoy et al.*, 2006; *Blume et al.*, 2009].

[4] Assessing and understanding spatial soil moisture variability has been a topic of active research for the past two decades [e.g., *Famiglietti et al.*, 1998]. Spatial soil moisture variability as a function of mean soil moisture content often shows a peak in the intermediate soil moisture range and lower variability at the wet and dry end in humid temperate climatic regions [e.g., *Lawrence and Hornberger*, 2007; *Pan and Peters-Lidard*, 2008]. The magnitude and location of the peak in soil moisture variability varies between ecosystems [*Western et al.*, 2003]. A multitude of controls on the soil moisture variability – mean soil moisture content relationship have been identified in previous studies: soil texture and structure [e.g., *Famiglietti et al.*, 1998; *Vereecken et al.*, 2007; *Pan and Peters-Lidard*, 2008], topography [e.g., *Grayson et al.*, 1997; *Nyberg*, 1996; *Famiglietti et al.*, 1998; *Vivoni et al.*, 2010], vegetation [e.g., *Teuling and Troch*, 2005], climate [*Lawrence and Hornberger*, 2007; *Teuling et al.*, 2007], and antecedent soil moisture [*Ivanov et al.*, 2010].

[5] The soil moisture variability – mean soil moisture content relationship is affected by soil properties including soil structure and texture because of their influence on soil hydraulic properties [see *Vereecken et al.*, 2007]. Under (very) wet conditions, soil moisture variability is mainly controlled by hydraulic conductivity and porosity [*Famiglietti et al.*, 1998; *Vereecken et al.*, 2007]. When the soil water in the catchment starts to drain and evapotranspire, the variability in saturated hydraulic conductivity, air entry pressure, and particle size distribution will lead to an increase in soil moisture variability [*Famiglietti et al.*, 1998; *Vereecken et al.*, 2007; *Pan and Peters-Lidard*, 2008]. When the soil moisture decreases to a threshold soil moisture (between wilting point and field capacity) the dominant process controlling drying switches from drainage to evapotranspiration [*Pan and Peters-Lidard*, 2008]. With further drying, soil moisture variability is diminished by evapotranspiration, which is positively correlated to soil moisture in dry soils [*Pan and Peters-Lidard*, 2008].

[6] Topography is also known to have a strong effect on soil moisture variability. *Grayson et al.* [1997] introduced a framework in which soil moisture patterns in (sub)humid temperate regions of Australia transit between two preferred states: the dry and wet state. They reported that the wet state is predominantly controlled by lateral water movement related to catchment terrain and denoted this as "nonlocal." In contrast, the dry soil moisture state is dominated by vertical fluxes such that soil properties and local terrain are the dominant (local) controls for spatial patterns. In areas with high relief energy, soil moisture variability is high and controlled by catchment terrain in wet conditions prior to rainfall [see, e.g., *Grayson et al.*, 1997; *Famiglietti et al.*, 1998] because convergent areas are wetter than divergent areas due to moisture accumulation associated with lateral water movement. After rainfall, the upslope areas will also be wetted, which leads to a reduction in soil moisture variability. With continued drying of the catchment, the importance of lateral flow processes diminishes and the nonlocal control of topography on the soil moisture variability is strongly reduced [*Western et al.*, 1999, 2003]. Instead, local controls, such as soil properties, start to dominate soil moisture variability [*Famiglietti et al.*, 1998].

[7] Soil moisture variability is also controlled by vegetation via root water uptake and throughfall patterns among other factors [*Fernandez-Illescas et al.*, 2001]. It is commonly assumed that soil moisture variability increases in relatively wet soil conditions due to spatially variable unstressed root water uptake, whereas soil moisture variability is assumed to decrease in dry soil conditions because of the greater ability of plants to take up water from regions in the soil that are still wet [*Bouten et al.*, 1992; *Teuling and Troch*, 2005; *Teuling et al.*, 2007; *Ivanov et al.*, 2010]. Strong control of evapotranspiration on soil moisture variability was detected in agricultural fields (maize) by *Hupet and Vanclooster* [2002] and pasture fields by *Western et al.* [1998]. Since root water uptake by trees is typically higher than uptake by crops, the control of root water uptake on soil moisture variability is expected to be larger in forests [*Schume et al.*, 2003]. In addition, spatial redistribution of precipitation due to canopy interception and associated leaf drip leads to heterogeneous throughfall patterns in forests [*Bouten et al.*, 1992; *Beier et al.*, 1993]. *Jost et al.* [2004] reported an increase of soil moisture variability in a spruce forest after rainfall due to heterogeneous throughfall. Also *Beier et al.* [1993] described spatially variable throughfall under spruce and found that throughfall increased with distance from the tree stem.

[8] More recently, *Vivoni et al.* [2010] observed clockwise event-scale hysteresis in soil moisture variability dynamics at 5 cm depth in a basin with elevation ranging from 660 to 1680 m, variable soil textures (sand to sandy clay loam), and four vegetation types (subtropical scrubland, oak savanna, grassland, and evergreen forest). *Vivoni et al.* [2010] argued that hysteresis loops in the $SD_\theta(\overline{\theta})$ dynamics are related to different sets of complex interacting factors that control the drying and wetting arms. Controls on the drying arm are vertical and lateral soil moisture redistribution and evapotranspiration, whereas precipitation, vegetation, infiltration, and soil moisture ($\overline{\theta}$) are the major controls in the wetting arm [*Jost et al.*, 2004; *Vivoni et al.*, 2010; *Ivanov et al.*, 2010]. *Jost et al.* [2004] suggested that the wetting response of spatial soil moisture patterns for low $\overline{\theta}$ in clayey soil under spruce was controlled by preferential flow and hydrophobicity. In contrast, the wetting response at intermediate $\overline{\theta}$ was determined by heterogeneous throughfall patterns because cracks are closed and hydrophobicity is lower [*Jost et al.*, 2004].

[9] Groundwater was found to be a major control that drives spatial soil moisture variability in the Shale Hills Critical Zone Observatory [*Takagi and Lin*, 2011]. At this site, a shallow groundwater table in the near-stream zone was seasonally present (dormant season/wet soil moisture state) or absent (vegetation period/dry soil moisture state) which affected both the mean soil moisture content and the spatial soil moisture variability.

[10] Most previous studies determined spatial soil moisture variability for a few selected times and the topsoil only. However, spatial soil moisture measurements at a limited number of times may not be adequate to infer the temporal dynamics of spatial soil moisture patterns [*Western et al.*, 2002] and to

generalize conclusions about spatial dependence [*Schume et al.*, 2003]. Moreover, little is known about the temporal dynamics of spatial soil moisture variability in small forested catchments [*Jost et al.*, 2005], particularly at short time scales (<1 day) during and directly after rainfall [*Jost et al.*, 2004] and at the seasonal to annual time scale. Obviously, recently developed wireless sensor networks [e.g., *Bogena et al.*, 2010] that continuously provide 3-D soil moisture data with a high temporal resolution, sufficient spatial coverage, and vertical resolution over the profile could contribute significantly to improving our process understanding of hydrological systems [e.g., *De Lannoy et al.*, 2006; *Robinson et al.*, 2008; *Vereecken et al.*, 2008].

[11] This study uses data from such a network and goes beyond recent research by characterizing both seasonal and event-scale dynamics at multiple depths in a forested catchment based on one year of hourly soil moisture data. Soil moisture data provided by the wireless sensor network SoilNet [*Bogena et al.*, 2010] were investigated by means of univariate and geostatistical analysis. The objectives of this study were: (1) to assess the feasibility of SoilNet to study short-term and long-term temporal variation in spatial soil moisture patterns; and (2) to investigate how dynamics of spatial patterns vary with depth, mean soil moisture content, season, and individual wetting and drying periods. The paper is organized as follows. First, the study site, soil moisture measurement techniques, and data analysis strategy are described (section 2). Then, the hydrological situation during the study period is presented (section 3.1). Following that we discuss the temporal dynamics of spatial soil moisture patterns at various depths (section 3.2), the dependence of soil moisture variability on mean soil moisture content at various depths (section 3.3), seasonal effects on topsoil spatial soil moisture variability and correlation (sections 3.4 and 3.5), the effect of wetting and drying processes on topsoil soil moisture variability at annual (section 3.6), and event time scales under different wetness states (section 3.7). Finally, our summary and conclusions are provided (section 4).

2. Materials and Methods

2.1. The Wüstebach Test Site

[12] The Wüstebach test site is part of the TERENO Eifel/Lower Rhine Valley Observatory in Germany [*TERENO*, 2011; *Zacharias et al.*, 2011]. The test site contains the headwater system of the river Wüstebach. It is a subcatchment of the river Rur basin and is situated in a low mountain range within the Eifel national park (50° 30′N, 6° 19′E, WGS84) (Figure 1). It has an area of 0.27 km^2 with a maximum N-S *extent* of 500 m and a maximum E-W *extent* of 800 m. The altitude increases from 595 m in the north to 628 m in the south, the mean slope is 3.6% with a maximum of 10.4% [*Bogena et al.*, 2010]. The bedrock consists of Devonian shales with sporadic sandstone inclusions, and is covered by a 1 to 3 m thick periglacial solifluction layer in which mainly Cambisols (soil type 1) in the western part and stagnic Cambisols (soil type 2) in the eastern part of the test site have developed. In the valleys, groundwater has a considerable influence and Planosols (soil type 3) are associated with Gleysols (soil type 4) and half-bogs (soil type 5) (Figure 1). Thus, both groundwater-distant (soil types 1 and 2) and groundwater-influenced soil types (soil types 3, 4, and 5) are present. The soil texture is silty clay loam with medium to very high fraction of coarse material [*Richter*, 2008]. The test site is located in the humid

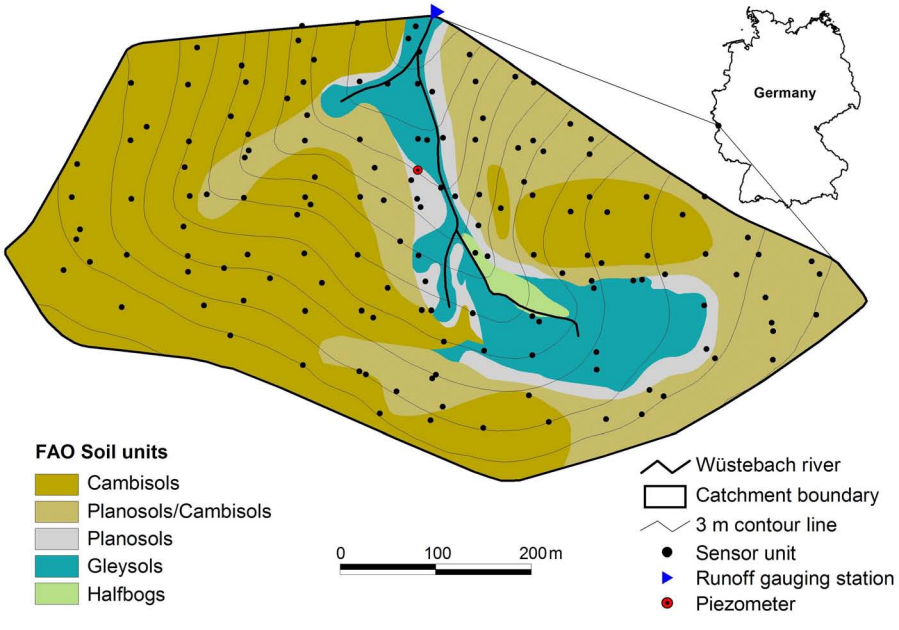

Figure 1. Map of the TERENO forest test site Wüstebach with isolines and soil types (ST1: Cambisol; ST2: Planosol/Cambisol; ST3: Planosol; ST4: Gleysol; and ST5: Halfbog; while ST1 and ST2 refer to groundwater-distant areas; whereas ST3, 4, 5 refer to groundwater-influenced areas) as well as measurement points (sensor units) of the wireless sensor network SoilNet. Measurement locations in ST1–ST2 are defined as groundwater distant, whereas those located in ST3–ST5 are defined as groundwater influenced.

temperate climatic zone with a mean annual precipitation of 1107 mm (1961–1990) and a mean annual temperature of 7°C [*Zacharias et al.*, 2011]. The main vegetation is Norway spruce (*Picea abis L.*), which was predominantly planted in 1946, and Sitka spruce (*Picea sitchensis Bong.*), which was mainly planted in 1949 [*Etmann*, 2009]. The growing season is approximately 130 days (from April/May to September/October).

2.2. Soil Moisture Measurements

[13] The soil moisture data were measured with the wireless sensor network SoilNet, which is described in detail elsewhere [*Bogena et al.*, 2010; *SoilNet*, 2011]. The sensor network in the Wüstebach test site consists of 150 end device units (measurement locations), each measuring a soil moisture profile, 18 router units and one coordinator unit (Figure 1). The sensor network was designed to support geostatistical analysis. Therefore, 74 out of 150 measurement locations are arranged on a 60 × 60 m grid to provide adequate spatial coverage and the remaining 76 measurement locations are randomly distributed to also sample small-scale variability. Using this strategy, there were 117 measurement locations in groundwater-distant soil types and 33 measurement locations in groundwater-influenced soil types. At each measurement location, soil moisture was measured at three depths (5, 20, 50 cm) using horizontally installed ECH2O sensors (EC-5 and 5TE, Decagon Devices Inc., Pullman, USA). Soil moisture data (θ, vol. %) were obtained from ECH2O sensor response measurements using a two-step-approach as detailed in Appendix A. A known drawback of these sensors is the small sampling volume [*Blonquist et al.*, 2005, *Cobos*, 2008]. To increase the measurement volume and to check for measurement quality, two sensors were installed at the same depth with a separation of only 0.05 m. At 5 and 50 cm depths, one EC-5 and one 5TE sensor were installed. At 20 cm depth, two EC-5 sensors were installed. Soil moisture measurements were made every 15 min, and these measurements were averaged to obtain hourly soil moisture data. The monitoring period analyzed in this study started on 1 August 2009 and ended on 31 July 2010.

2.3. Outlier Detection

[14] In a wireless sensor network application, data loss occurs for various reasons and, therefore, the number of measurements available for a particular time and depth is variable (Figure 2). On some occasions, the number of measurements at a particular time was reduced because end device units or router units did not perform properly (e.g., due to low battery voltage), and increased again after periodic maintenance (e.g., battery exchange). It was also observed that the number of available measurements was lower during wet periods (e.g., in autumn 2009). This was related to signal attenuation, which affected data communication between end device units and router units [e.g., *Bogena et al.*, 2009]. The average number of available measurements at a particular time also varied with depth and was lower for 5 and 50 cm depth. This is related to the 5TE sensors installed at these depths, which were more prone to sensor failure. In order to reduce data loss and to avoid that outliers would affect the (geo)statistical analyses, the available soil moisture measurements were inspected for outliers in three steps: (1) qualitative plausibility checks, (2) quantitative plausibility checks, and (3) a spatial outlier test. In the first step, the plausibility of the soil moisture data was checked qualitatively. For example, sensors with high noise were completely removed. In the second step, quantitative plausibility checks were also performed for the time series of each individual sensor at the original resolution of 15 min. This included that soil moisture data were marked for one of the three treatment options if the actual soil moisture value was outside the range of 0 to 100 vol. %. First, a substitution was attempted in which the soil moisture value provided by the other sensor in the same depth was used if this value had a difference less than ±5 vol. % with the two previous measured soil moisture contents. If substitution was not successful, linear interpolation between the previous and the following soil moisture value was attempted. Again, this interpolated value was only accepted when the difference with the two previously measured values (i.e., during the previous 30 min) was less than ±5 vol. %. If both substitution and interpolation were unsuccessful, the data point was removed from the data set thus leading to data

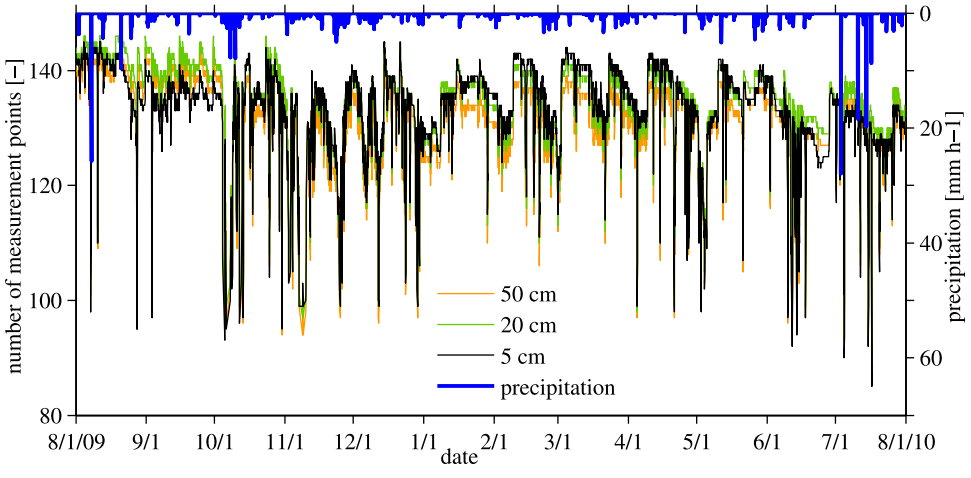

Figure 2. Time series of the number of measurements (end device units) at 5, 20, and 50 cm depths as well as the time series of precipitation.

loss. Only about 0.8% of the data were removed by this procedure. To ensure sufficient spatial coverage at all times, all hourly data sets with less than 100 sampling locations for a particular depth were discarded. In the third and final test, a slightly simplified spatial outlier test following *Chen et al.* [2008] and *Kou* [2006] was performed. Spatial outliers were identified and removed when the difference between the local value and the distance-weighted average within a 100 m radius was larger than 25 vol. %. This affected between 1% and 2% of the data.

2.4. Separation Into Seasonal and Event Time Scales

[15] In this paper we analyzed the dynamics of spatial soil moisture variability and patterns on various temporal scales. Therefore, the 1 year long soil moisture data set was separated into (1) seasonal and (2) event (wetting-drying-periods) data sets. The seasonal data sets (summer 2009, autumn 2009, winter 2009/10, spring 2010, and summer 2010, dates are provided in Table 2) represent changes in weather (temperature, evapotranspiration, snow melting) and phenology over the year. Each season was composed of multiple complete wetting-drying periods (WDP). These were separated by assuming that a wetting period started with a precipitation event that resulted in an increase of the mean soil moisture of at least 2 vol. % and lasted at least 24 h.

2.5. Statistical Analysis

[16] The 4-D soil moisture data set was first investigated using univariate descriptive statistical analysis. The spatial mean soil moisture ($\overline{\theta}$) and soil moisture variability (expressed as the standard deviation SD_θ) were estimated for each time and depth (5, 20, 50 cm) using the standard sample estimators. In the next step, spatial soil moisture patterns were investigated using geostatistical analysis. Spatial autocorrelation was quantified using the omnidirectional experimental semivariance:

$$\hat{\gamma}(h) = \frac{1}{2N(h)} \sum_{i=1}^{N(h)} (\theta_i - \theta_{i+h})^2, \quad (1)$$

where $N(h)$ is the number of data pairs within a given distance class, θ_i is the soil moisture at location i, and θ_{i+h} is the soil moisture at locations separated from i by distances h that fall within the distance class. Semivariance was calculated using the *gamv* algorithm of GSLib [*Deutsch and Journel*, 1998]. A fixed number of seven lags with a lag class width of 40 m was used (i.e., lag classes were 20–60 m, 60–100 m, . . ., 260–300 m). Additionally, the semivariance between the two sensors installed at one node at the same depth was considered as the first lag with a separation distance of 0.05 m. This was done to ensure an appropriate estimation of the nugget variance. The number of data pairs at various lags changed (between 140 and 300 m they decreased from 738 to 305 for 5 cm, from 1114 to 446 for 20 cm, and from 1057 to 409 for 50 cm depths) because the number of measurements varied with time and depth (see also Figure 2). For interpretation of the estimated experimental semivariance, scaling effects have to be considered [see *Western and Blöschl*, 1999]. According to *Western and Blöschl* [1999], an increase in measurement support (measurement averaging scale) will result in a decrease in variability; an increase in extent (size of the field site) will result in an increase in variability, whereas a change in spacing (distance between measurements) will not affect variability. An exponential variogram model was used consistently since it generally provided the best fits:

$$\gamma(h) = c_0 + c_1 \left[1 - \exp\left(-\frac{3h}{a}\right)\right], \quad (2)$$

where h is the lag separation distance, c_0 is the nugget, c_1 is the structural semivariance, and a is the *range*, which is three times the spatial autocorrelation length for the exponential variogram model. The nugget c_0 results from subscale spatial variability and measurement error. The total sill $(c_0 + c_1)$ characterizes the semivariance at which the variogram flattens out. We further refer to the nugget effect as the ratio between the nugget variance and the total sill $[=c_0/(c_0 + c_1)]$. The *range* indicates the maximum distance of spatial autocorrelation and is a measure of spatial continuity [*Western and Blöschl*, 1999]. To estimate the variogram, the exponential model (equation (2)) was automatically fitted to the experimental semivariance values (equation (1)) using the nonlinear fitting algorithm *lsqcurvefit* from MatLab (Mathworks, Nutick, USA). A selection of variogram fits was examined visually to check the integrity of the fitting algorithm. The goodness-of-fit was quantified by the coefficient of efficiency R^2 [*Nash and Sutcliffe*, 1970]. *Ordinary kriging* was performed with the *kt3d* algorithm of GSLib [*Deutsch and Journel*, 1998] to obtain spatially interpolated soil moisture maps.

[17] In order to avoid situations where first-order stationarity is nonexistent, we excluded catchment scale nonstationary data from the geostatistical analysis (indicated by ranges larger than 300 m, which is about half of the catchment extent).

3. Results and Discussion

3.1. Hydrological Characteristics of the Measurement Period

[18] The data sets used in this study (including soil moisture, meteorological, groundwater, and runoff data) are freely available via the TERENO data portal (www.tereno.net). The annual time series of air temperature, open-field rainfall, and snow from a nearby weather station (~3 km north-east) are presented in Figure 3a. Measured runoff and groundwater levels are shown in Figure 3b. The spatial mean soil moisture ($\overline{\theta}$) at 5, 20, and 50 cm depths are provided in Figure 3c. To simplify interpretation, we arbitrarily distinguish in the following three soil moisture states based on visual interpretation of the SD_θ–$\overline{\theta}$ relationship presented later (see Figure 7): a dry state ($\overline{\theta}_{5cm} < 30$ vol. %), an intermediate state ($30 < \overline{\theta}_{5cm} < 47$ vol. %) and a wet state ($\overline{\theta}_{5cm} > 47$ vol. %). Table 1 provides annual and seasonal summary statistics. In the following we briefly highlight the main hydrological events during the study period.

[19] At the beginning of August 2009, a large precipitation event of 26 mm occurred when the topsoil $\overline{\theta}$ was in the intermediate state (38 vol. %). This event resulted in rapid increase of the topsoil $\overline{\theta}$ and produced runoff (peak flow at the gauging station of 0.17 mm) indicating that lateral

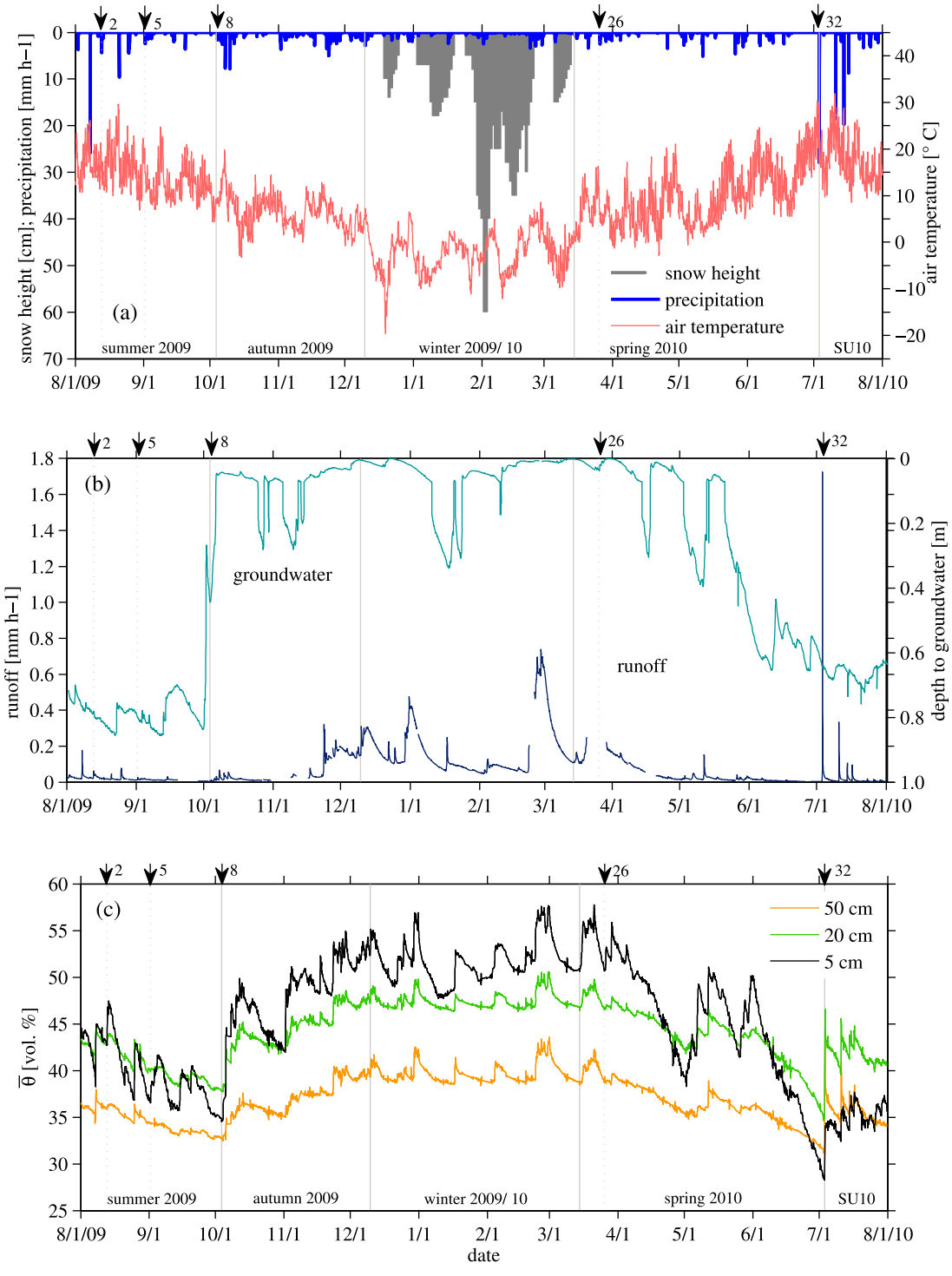

Figure 3. Time series (1 August 2009–31 July 2010) of (a) daily snow height (climate station Kalterherberg), hourly precipitation, and hourly air temperature (station meteomedia/Schleiden-Schöneseiffen), (b) hourly runoff (station Wüstebach), hourly groundwater of one gauge, and (c) hourly mean soil moisture ($\overline{\theta}$) at 5, 20, and 50 cm depths (measured by SoilNet). Gray lines indicate seasonal separation (dates are provided in Table 1) and black arrows indicate the beginning of selected wetting periods, respectively.

redistribution processes were activated. Later in the summer of 2009, only short-term changes in the topsoil $\overline{\theta}$ were observed, whereas only small short-term and long-term changes in subsoil $\overline{\theta}$ and small runoff were noticeable despite a range of precipitation events with a total precipitation amount of 90 mm in August and 44 mm in September. This indicates that a large part of the resulting soil water was lost through evaporation and root water uptake in

Table 1. $\overline{\theta}$ and Mean SD_θ for 5, 20, and 50 cm Depth Estimated for the Annual (Additionally Also the Maximal $\overline{\theta}$) and for Each Seasonal Data Set

	5 cm		20 cm		50 cm	
	$\overline{\theta}$	SD_θ	$\overline{\theta}$	SD_θ	$\overline{\theta}$	SD_θ
Data Set[a]	(vol. %)					
Year	45.7	11.9	44.2	9.6	37.0	8.9
	$\overline{\theta}_{max} = 57.7$		$\overline{\theta}_{max} = 50.6$		$\overline{\theta}_{max} = 43.7$	
SU 09	39.8	13.6	40.7	10.6	34.5	9.1
AU 09	48.3	11.8	44.8	9.8	37.2	9.2
WI 09/10	51.7	10.7	47.4	9.0	39.7	9.1
SP 10	45.3	11.6	43.8	9.5	36.5	8.6
SU 10	35.1	13.3	41.8	9.9	35.6	8.3

[a]The seasonal data sets, separated as mentioned in section 2.4, were summer 2009 (SU 09: start of the monitoring period 1 Aug 2009 12 am to 3 Oct 2009 6 pm), autumn 2009 (AU 09: 3 Oct 2009 6 pm to 9 Dec 2009 10 pm), winter 2009/10 (WI 09/10: 9 Dec 2009 10 pm to 14 Mar 2010 5 pm), spring 2010 (SP 10: 14 Mar 2010 5 pm to 3 Jul 2010 1 pm) and summer 2010 (SU 10: 3 Jul 2010 1 pm to the end of the monitoring period 31 Jul 2010 11 pm).

20 and 50 cm and that no significant lateral flow occurred. For a spruce forest with similar soil moisture content, *Jost et al.* [2004] also reported that low to medium precipitation events resulted in topsoil water recharge only.

[20] At the beginning of autumn 2009, the average temperature decreased to 8°C and the evapotranspiration demand decreased accordingly. In early October, several rainfall events (in total ~60 mm) led to a rapid increase of soil moisture in the entire soil profile. The groundwater level increased as well, but runoff did not respond strongly. Numerous precipitation events in November and December 2009 (total 210 mm) further increased $\overline{\theta}$ and filled the groundwater body, which resulted in fast rainfall-runoff responses.

[21] Winter 2009/10 was dominated by snow accumulation and snowmelt. The temperature dropped below 0°C in December 2009 and the first of four snow events occurred. In the presence of snow cover, $\overline{\theta}$ decreased. Subsequent snow melt events increased $\overline{\theta}$ in the entire soil profile. Once the soil was completely saturated (e.g., 1 January 2010 and 1 March 2010), high runoff indicated that snow melt also resulted in lateral surface runoff and fast subsurface flow.

[22] In spring 2010, the temperature and evapotranspiration rates increased again. Combined with only 17 mm precipitation in April this resulted in a strong decrease in $\overline{\theta}$ of the topsoil. Precipitation in May was 90 mm, so that topsoil $\overline{\theta}$ increased again. In contrast, precipitation in June 2010 was only 23 mm and the high evapotranspiration rates resulted in a strong decrease of $\overline{\theta}$ at all three depths and the lowest $\overline{\theta}$ of the study period occurred. The groundwater level also decreased distinctly during this period (Figure 3b).

[23] In early summer 2010, intense precipitation (Figure 3a) on relatively dry topsoil resulted in an abrupt and distinct increase of mean soil moisture in the subsoil (20 cm: from 35 to 47 vol. %; 50 cm: from 31 to 44 vol. %), whereas the response of the topsoil moisture content was also rapid but smaller (from 28 to 33 vol. %). The associated rapid runoff-response indicates that a large portion of the rainfall water bypassed the topsoil possibly due to preferential flow in soil cracks, as already described by *Zacharias et al.* [2011] and detailed further in section 3.7.3 (see also Figure 15 and Table 4).

[24] In summary, $\overline{\theta}$ in the Wüstebach test site generally decreased with depth during the dormant season. After a prolonged drying phase in late spring 2010, $\overline{\theta}$ at 5 cm depth was less than at 20 and 50 cm depths during most of summer 2010. Only $\overline{\theta}$ at 5 cm depth reached all three soil moisture states, whereas $\overline{\theta}$ at 50 cm depth stayed in the intermediate state permanently. We assume that the maximal soil moisture in 20 and 50 cm depths is likely to be lower related to higher bulk density and lower porosity in deeper depths (data not available). The temporal changes in $\overline{\theta}$ were strongest at the 5 cm depth, presumably because the topsoil is more strongly subject to climate forcing. Temporal changes in $\overline{\theta}$ at 20 and 50 cm depths were mostly smaller. This indicates that soil water redistribution and root water uptake processes reduced temporal $\overline{\theta}$ dynamics in the subsoil. The transition times between $\overline{\theta}$ states in the topsoil varied. The transition from the wet to the dry state (drying) was slow in summer 2009 (2 months). This long period in the intermediate $\overline{\theta}$ state in summer 2009 was caused by the balance between precipitation and evaporative demand. Several precipitation events interrupted drying periods, thus soil moisture varied within a range of 35 to 47 vol. % (see Figure 3c). The transition from the wet to the dry state (drying) in spring 2010 was faster (1 month) and the transition from the dry end of the intermediate state to the wet state (wetting) in autumn 2009 occurred quickly (within 1 week).

3.2. Temporal Dynamics of Spatial Soil Moisture Patterns at Various Depths

[25] Dynamic soil moisture probability distributions were observed. In wet and dry conditions bounding effects caused negatively and positively skewed distributions, respectively (not shown). During drying, bimodal distributions were sometimes observed, which have also been noted by *Vivoni et al.* [2010]. During intermediate soil moisture conditions the distribution was symmetric and close to normal. Despite these variations in shape, the spread was always reasonably represented by the standard deviation because the skew never became particularly extreme in either direction.

[26] The temporal dynamics of spatial soil moisture variability (quantified by the standard deviation SD_θ) for all measurement depths are presented in Figure 4. Several summary statistics are provided in Table 1. The mean SD_θ decreased with depth (from 11.8 to 9.6 to 8.9 vol. %). However, the SD_θ variation with depth changed seasonally. In the summer months there was a strong reduction in SD_θ with depth. In autumn and winter mean SD_θ was similar for 20 and 50 cm, while the topsoil SD_θ was typically higher and more dynamic (Figure 4). The SD_θ at 20 cm depth showed similar but less pronounced temporal behavior compared with SD_θ at 5 cm depth, whereas SD_θ at 50 cm depth was relatively constant. This agrees with findings by others [e.g., *Hupet and Vanclooster*, 2002; *Takagi and Lin*, 2011] who observed greatest temporal changes in topsoil spatial soil moisture variability and a decreasing trend with depth. SD_θ depends on mean soil moisture content, as will be discussed in more detail in section 3.3.

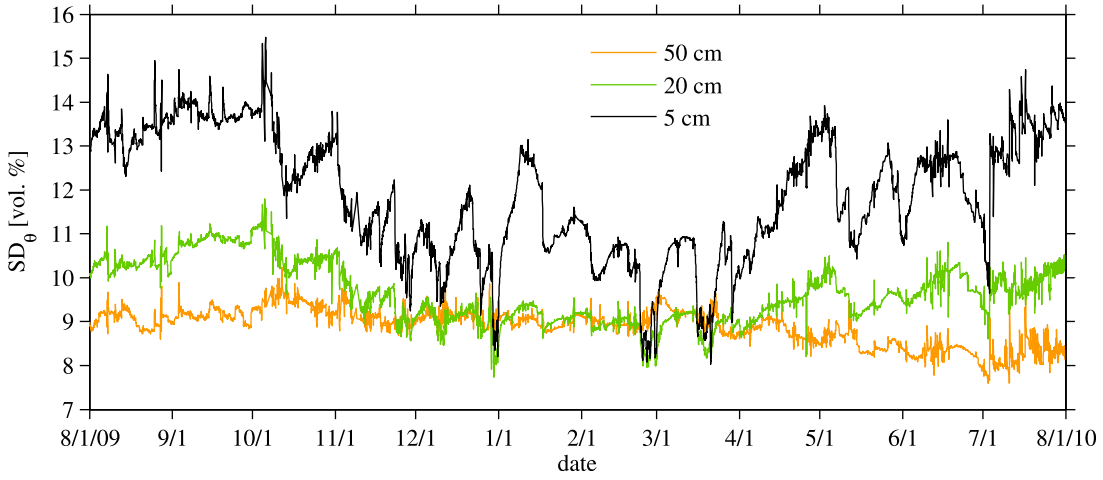

Figure 4. Time series (1 August 2009 to 31 July 2010) of soil moisture variability (standard deviation, SD_θ) at 5, 20, and 50 cm depths.

[27] The temporal dynamics of the fitted variogram model parameters (nugget, sill, and range) is shown in Figure 5 for all measurement depths. The quality of fit between the exponential variogram model and experimental semivariance data was very good for all depths (mean $R^2 > 0.90$). The goodness-of-fit of the variogram models was consistent throughout the year, with the exception of the topsoil where lower R^2 values were found in the dormant season

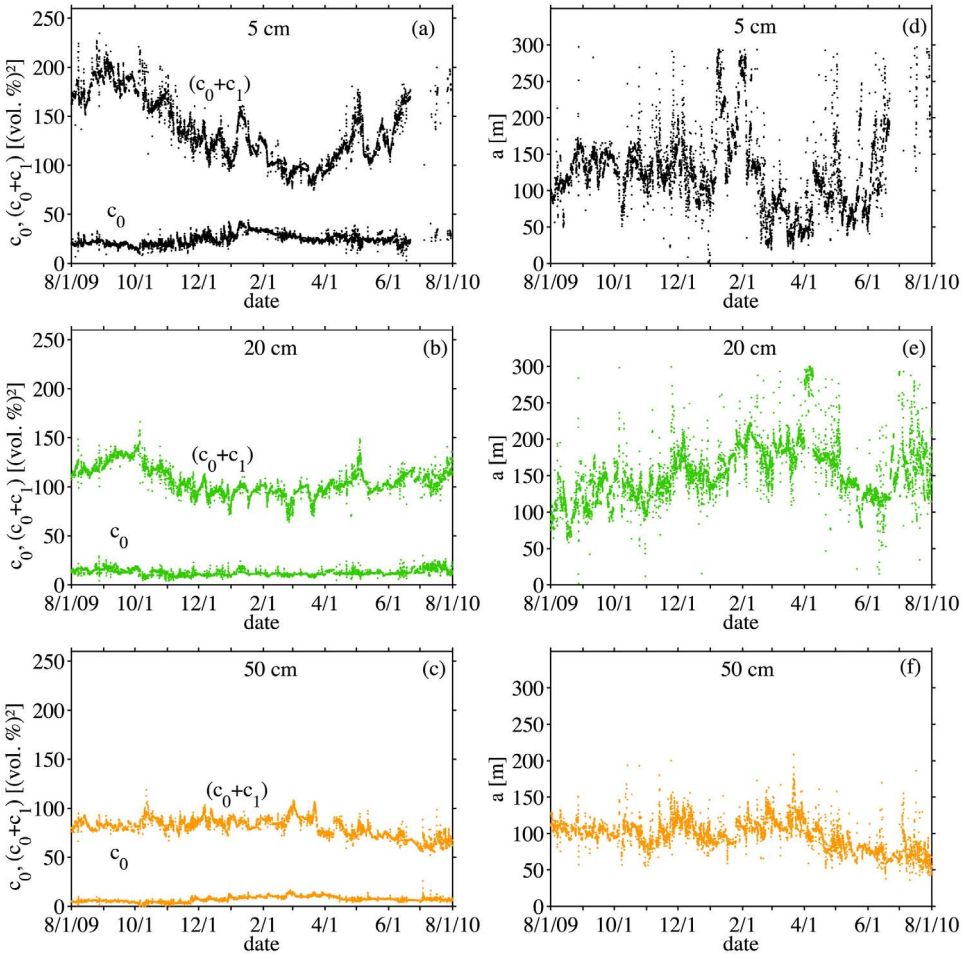

Figure 5. Time series of the nugget (c_0, lower curves) and the total sill ($c_0 + c_1$, upper curves) at depths of (a) 5 cm, (b) 20 cm, and (c) 50 cm, and (d, e, f) the variogram range (a) at depths of 5, 20, and 50 cm, respectively.

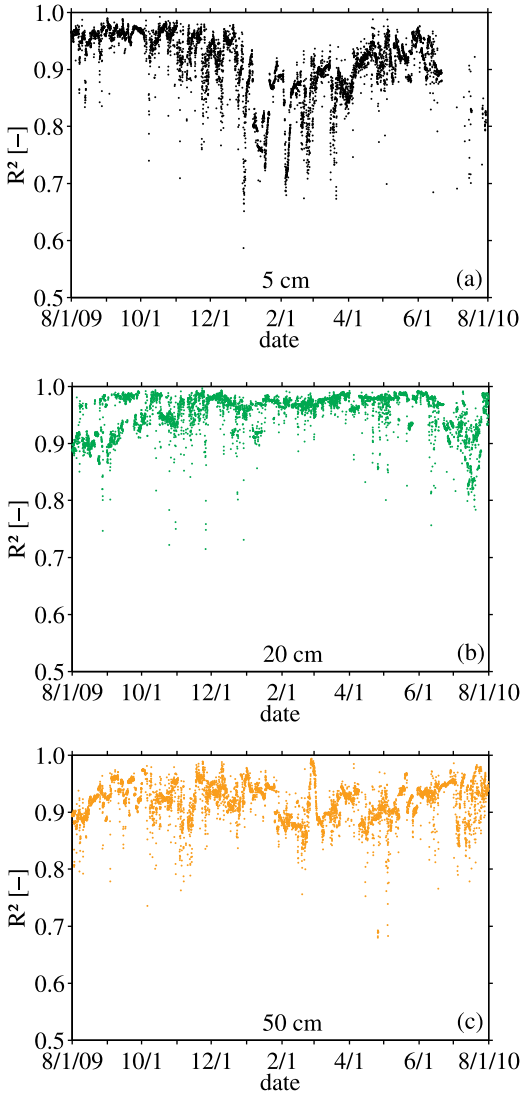

Figure 6. Time series of goodness of fit between experimental variogam and exponential variogram model R^2 at (a) 5 cm, (b) 20 cm, and (c) 50 cm depths.

(wet soil moisture state) (Figure 6). As expected, the total sill and SD_θ showed very similar behavior with depth and time. The nugget and the nugget effect were relatively low for all depths indicating reasonably low measurement errors and small-scale variability (separation <5 cm) in comparison to the total sill (Figures 5a–5c). This may have been affected to some degree by the procedure used to treat outliers, however only about 0.8% of data were affected by the procedure (see section 2.3). It should also be remembered that we used pairs of sensors separated by 5 cm to estimate the nugget rather than extrapolating from more widely spaced data, which we believe greatly improves the nugget estimation. The mean nugget decreased with depth from 25 to 12 and to 7 (vol. %)^2. The nugget was rather constant at 20 cm depth, while the nugget was more variable for the 5 and 50 cm depths, especially during periods with high $\overline{\theta}$ (dormant season).

[28] The mean variogram range for the 5 cm depth was 123 m, whereas it was longer (159 m) for the 20 cm depth, but shorter at the 50 cm depth (96 m) (Figures 5d–5f). In addition, the range was more variable in time in the topsoil than in the subsoil. This is directly related to the meteorological forcing that most strongly influences the topsoil $\overline{\theta}$. Ranges larger than 300 m were observed mainly in summer 2010. Such large ranges can be explained by a pronounced spatial organization as a result of relatively dry upslope areas contrasting with relatively high soil moisture at the valley mainly due to the influence of a shallow groundwater table. This persisting contrast becomes larger when $\overline{\theta}$ decreases and at some point the nonstationarity becomes distinct. Unfortunately, this complex nonstationarity cannot be easily taken into account since only rather weak correlations ($R^2 < 0.16$) between soil moisture and elevation, slope and wetness index for the Wüstebach catchment have been found [*Bogena et al.*, 2010]. Instead, in order to reduce the effect of nonstationary, the situations where range values exceeded 300 m were discarded and not used for further interpretation. Despite the possibility that still some nonstationarity might exist in the data, semivariance analyses gave a reasonable description of the spatial structure of the catchment for range values below 300 m. Therefore, we assume that the contribution of a deterministic spatial trend resulting from the catchment topography and the underlying spatial pattern of soil types is likely to be very small for the determined variograms and mainly affects the large distance semivariances.

3.3. Linking Spatial Soil Moisture Variability to Mean Soil Moisture at Various Depths

[29] It has often been reported that spatial soil moisture variability is linked to $\overline{\theta}$ [e.g., *Western et al.*, 2003]. To investigate this, the soil moisture variability expressed as SD_θ as a function of $\overline{\theta}$ [i.e., $SD_\theta(\overline{\theta})$] is presented for 5, 20, and 50 cm (Figure 7). $SD_\theta(\overline{\theta})$ was distinctly different for the three depths and was most pronounced at the intermediate $\overline{\theta}$ state. $SD_\theta(\overline{\theta})$ for the topsoil showed a convex shape that has been reported repeatedly for soil moisture variability at the catchment scale [e.g., *Western et al.*, 2003; *Ryu and Famiglietti*, 2005; *Teuling and Troch*, 2005; *De Lannoy*, 2006; *Choi and Jacobs*, 2007; *Lawrence and Hornberger*, 2007]. $SD_\theta(\overline{\theta})$ peaked in the intermediate soil moisture state at a critical soil moisture ($\overline{\theta}_{crit}$) for the 5 and 20 cm depths (Figure 7). No distinct peak was evident at 50 cm depth. Fitting a third-order polynomial function to the topsoil data presented in Figure 7 ($R^2 = 0.91$) led to a $\overline{\theta}_{crit}$ of 39.3 vol. % and a $SD_{\theta,max}$ of 13.5 vol. %. It is also worth noting that the scatter in $SD_\theta(\overline{\theta})$ was largest in the intermediate $\overline{\theta}$ state. In the wet range, variation in $SD_\theta(\overline{\theta})$ was much lower. At the dry end, scatter in $SD_\theta(\overline{\theta})$ was not observed because the dry state was only reached during a single drying period at the end of June 2010 (Figure 3c). The scatter in $SD_\theta(\overline{\theta})$ was particularly evident in the topsoil, as also observed by *Famiglietti et al.* [1998], among others.

[30] The bound of $SD_\theta(\overline{\theta})$ at the wet end decreased with depth due to decreasing porosity associated with decreasing organic matter content. The remaining soil moisture variability at the highest $\overline{\theta}$ is largely controlled by porosity variations within and between soil types, as was also suggested by *Famiglietti et al.* [1998] and *Teuling and Troch* [2005]. $SD_\theta(\overline{\theta})$ increases as soil moisture decreases from the highest

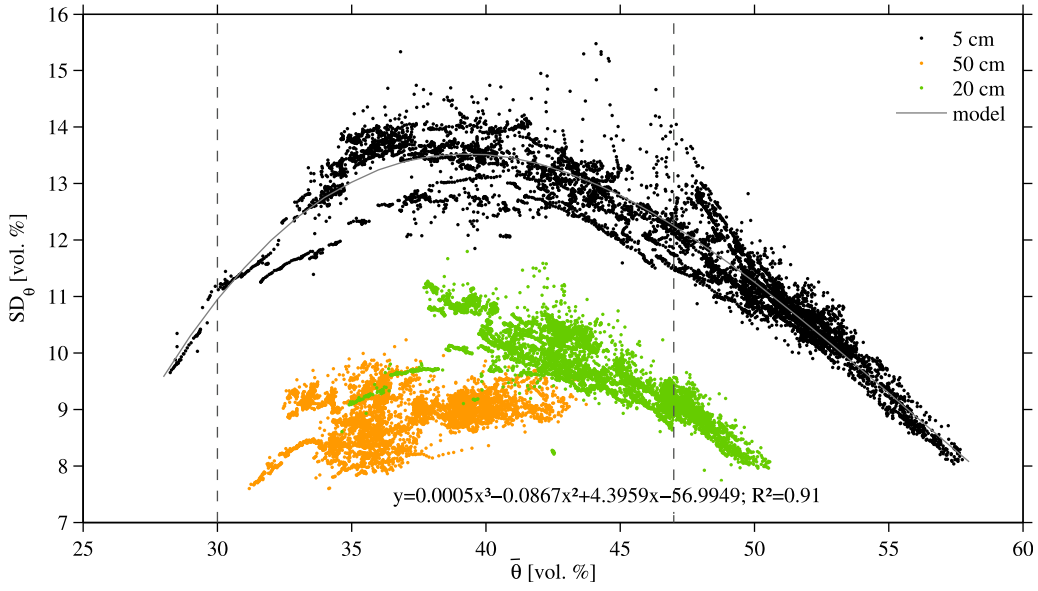

Figure 7. Standard deviation as function of mean soil moisture [$SD_\theta(\overline{\theta})$] at 5, 20, and 50 cm depths for the 1 year data set and a fitted third-order polynomial function to the topsoil data set.

$\overline{\theta}$. In wet soils, moisture is not a limiting factor on evapotranspiration and therefore the impact of vegetation on soil moisture variability is considered to be minor at the upper end of the wet range. Instead, soil moisture variability is mainly controlled by vertical and lateral water flow processes, i.e., coarser soils in upslope areas dry faster than more fine-textured soils in convergent areas [e.g., *Grayson et al.*, 1997; *Vereecken et al.*, 2007; *Pan and Peters-Lidard*, 2008]. As $\overline{\theta}$ dries toward $\overline{\theta}_{crit}$, drainage, evaporation, and root water uptake increase soil moisture variability. Below $\overline{\theta}_{crit}$, soil moisture variability in humid regions is mainly controlled by the limited water availability for evaporation and root water uptake. Since both are positively correlated with $\overline{\theta}$, higher evaporation and root water uptake from wet areas as compared to dry areas will lead to a decrease of soil moisture variability with decreasing $\overline{\theta}$ [*Pan and Peters-Lidard*, 2008; *Schume et al.*, 2003]. Additionally, the difference in SD_θ ($\overline{\theta}$) between depths was most pronounced at the intermediate $\overline{\theta}$ state since the effective redistribution by vertical flow, lateral flow, and evapotranspiration is strongest in this range. Other studies identified soil texture as the main control on $SD_\theta(\overline{\theta})$ at the dry end [see *Western et al.*, 2003; *Famiglietti et al.*, 1998; *Schume et al.*, 2003]. Because the Wüstebach catchment did not dry completely in the study period, it seems unlikely that the observed soil moisture variability can be attributed to soil texture only. Other controls, such as root water uptake and relict effects of lateral drainage, might still be influential because the water content has not decreased below the permanent wilting point.

[31] Groundwater also influences $SD_\theta(\overline{\theta})$ in the Wüstebach catchment. To investigate this, $SD_\theta(\overline{\theta})$ is presented separately for groundwater-distant (soil types 1, 2, see Figure 1) and groundwater-influenced areas (soil types 3, 4, 5, see Figure 1) [referred to as $SD_{\theta,GWd}(\overline{\theta}_{GWd})$, $SD_{\theta,GWi}(\overline{\theta}_{GWi})$ respectively, see Figure 9b]. As expected, $\overline{\theta}_{GWi}$ in groundwater-influenced areas was greater than $\overline{\theta}_{GWd}$ in groundwater-distant areas ($\overline{\theta}_{GWi}$ = 60 vol. % and $\overline{\theta}_{GWd}$ = 42 vol. %, respectively). In general, groundwater-distant areas showed more dynamic soil water than groundwater-influenced areas (Figure 8), as also emphasized by *Lin et al.* [2006]. The difference between $\overline{\theta}_{GWi}$ and $\overline{\theta}_{GWd}$ changed with time and was lower in winter (Figure 8). $\overline{SD}_\theta$ for the groundwater-influenced areas was higher than for the groundwater-distant soil types ($\overline{SD}_{\theta,GWi}$ = 10 and $\overline{SD}_{\theta,GWd}$ = 9 vol. %, respectively, see Figure 9b). This was attributed to variation of the groundwater level in spring and summer, which temporarily caused saturated regions near the stream that disappeared after some time but increased SD_θ. It is evident that the presence of the groundwater body near the stream increased both $\overline{\theta}$ and SD_θ (see Figure 9b).

3.4. Seasonal Effects on the Relation Between Soil Moisture Variability and Mean Soil Moisture of the Topsoil

[32] The temporal dynamics of spatial soil moisture patterns were most pronounced in the topsoil (Figures 4 and 5); for this reason we focus here on seasonal effects at 5 cm depth. The 1 year topsoil $SD_\theta(\overline{\theta})$ separated by season is presented in Figure 9a.The 1 year topsoil $SD_\theta(\overline{\theta})$ separated by both season and groundwater-influence is presented in Figure 9b. Seasonal differences in $SD_\theta(\overline{\theta})$ are mainly attributed to different wetness states of the Wüstebach catchment, with higher $\overline{\theta}$ during the dormant period (autumn 2009, winter 2009/10) reducing $SD_\theta(\overline{\theta})$. In the intermediate $\overline{\theta}$ range, SD_θ was lower in spring 2010 as compared with the other seasons (Figure 9b). Again, third-order polynomial functions were fitted to the data of spring 2010 (R^2 = 0.94) and to all other data (R^2 = 0.95). This led to a $SD_{\theta,max}$ of 12.9 vol. % at $\overline{\theta}_{crit}$ = 39.7 vol. % in spring 2010 compared with a $SD_{\theta,max}$ of 13.8 vol. % at $\overline{\theta}_{crit}$ = 38.9 vol. % for the other seasons. Interestingly, no seasonal difference in SD_θ in the intermediate $\overline{\theta}$ range was observed within groundwater-distant upslope areas (Figure 9b),

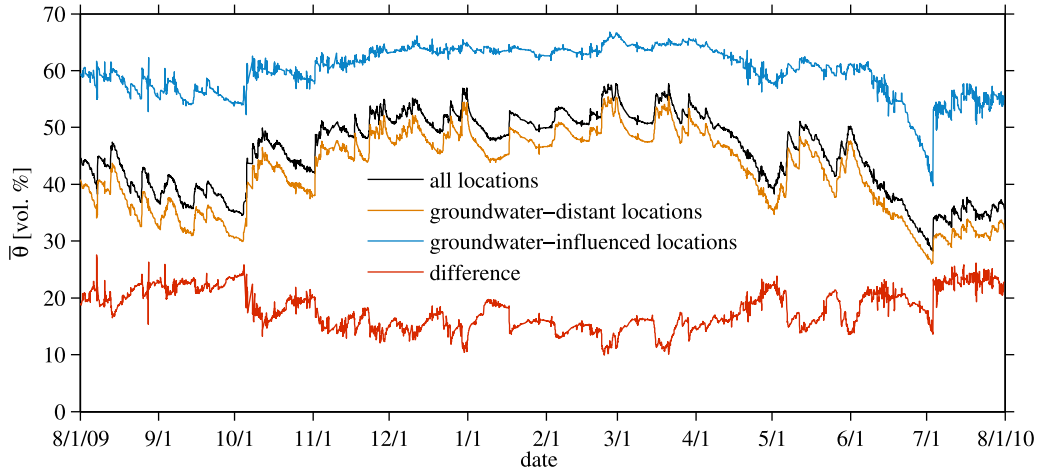

Figure 8. Time series of $\overline{\theta}$ for measurement points in all soil types (black), solely groundwater-distant soil types (brown, $\overline{\theta}_{GWd}$), solely groundwater-influenced soil types (blue, $\overline{\theta}_{GWi}$), and the difference between $\overline{\theta}$ of groundwater-influenced and groundwater-distant soil types (red) for the topsoil.

which suggests that the seasonal $SD_\theta(\overline{\theta})$ dynamics are related to contrasts between groundwater-distant upslope soils and groundwater-influenced soils at the valley bottom (i.e., contrasts at the larger spatial scale).

[33] Compared with summer 2009, the seasonal transition from the wet to dry state in spring 2010 (one drying event only, Figure 2c) was associated with a lower SD_θ (Figure 9a). In the groundwater-influenced sites, SD_θ mostly increases with decreasing $\overline{\theta}$ (Figure 9b), while this changes only at the end of the drying event in spring 2010 (Figure 9b). In contrast, a decrease of $\overline{\theta}$ in summer 2009 led to an increase of SD_θ (Figure 9a) because $\overline{\theta}$ in the groundwater-influenced areas remained high. Furthermore, the data from summer 2010 seem to line up again with data from summer 2009 (Figure 9a). Intense precipitation on relatively dry topsoil causes an increase in SD during the wetting transition in early 2010 [large positive $SD_\theta(\overline{\theta})$ gradient]. This rainfall bypassed the topsoil in the drier upslope area, but filled the moderately wet topsoil in the valley bottom; thus increasing catchment scale SD_θ rapidly and $\overline{\theta}$ moderately. Additionally, the SD_θ at the beginning of autumn 2009 (wetting transition) was also high due to controls (e.g., precipitation, vegetation, and groundwater) that enhanced the emergence of clockwise event-scale $SD_\theta(\overline{\theta})$ hysteresis. Both events will be described in detail later (see section 3.7). The data presented above suggest a clockwise seasonal $SD_\theta(\overline{\theta})$ hysteresis; however, some care is required with this interpretation given that only one annual cycle is considered here. Taken together, this indicates that hillslope scale lateral redistribution through groundwater is important in this seasonal scale $SD_\theta(\overline{\theta})$ behavior.

3.5. Linking Spatial Correlation Length to Mean Soil Moisture and Soil Moisture Variability in the Topsoil

[34] Figure 10a shows the variogram range as a function of mean soil moisture and Figure 10b shows the range as a function of the total sill for the topsoil separated by season. Nonstationary situations indicated by a range larger than 300 m were excluded from the analysis. It can be seen that the range increased as $\overline{\theta}$ decreased, except for autumn 2009. The increasing range with decreasing soil moisture is mainly attributed to the smoothing effect of evapotranspiration.

[35] During autumn 2009 the range varied around a mean of 135 m in the intermediate soil moisture range. The variability in range increased at the end of autumn in the transition to the wet $\overline{\theta}$ state (Figure 10a). This indicates that the range was relatively constant within this season, whereas the soil moisture variability as expressed by the total sill was changing (Figure 10b). Thus, precipitation (indicated by increasing $\overline{\theta}$) and soil moisture redistribution processes (indicated by decreasing $\overline{\theta}$) had only small effects on the spatial correlation length.

[36] In the wet $\overline{\theta}$ state, both the range and the total sill decreased with increasing $\overline{\theta}$ during winter 2009/10 (Figure 10a). Thus, a positive correlation between range and total sill was observed (Figure 10b). Below snow cover, soil moisture redistribution continued because the soil was unfrozen, which led to decreasing $\overline{\theta}$, increasing total sills, and increasing ranges. After snow melt, the soil wetted up quickly and surface lateral redistribution processes were activated, as evidenced by a large runoff event (Figures 3a and 3b). This lateral redistribution and the physical upper limits provided by the soil properties resulted in low total sills and ranges.

[37] The range and the total sill increased again during spring 2010 with decreasing $\overline{\theta}$ (Figures 10a and 10b). Both low and high range and total sill values occurred in the transition from the wet to the intermediate $\overline{\theta}$ state. An increasing range with increasing total sill was also observed. This was related to the fact that in the wet $\overline{\theta}$ state, both range versus $\overline{\theta}$ and total sill versus $\overline{\theta}$ increased with decreasing $\overline{\theta}$. The total sill in spring was on average slightly higher than in winter, whereas the ranges of both periods varied between low and high values. This indicates that spatial soil moisture patterns smoothed out (increasing range) and became more heterogeneous (increasing total sill) with soil drying.

3.6. Wetting-Drying Effects on the Relationship Between Topsoil Soil Moisture Variability and Mean Soil Moisture

[38] To further investigate the variability of $SD_\theta(\overline{\theta})$ for a given $\overline{\theta}$ (Figures 7 and 9a), we split the topsoil data set shown

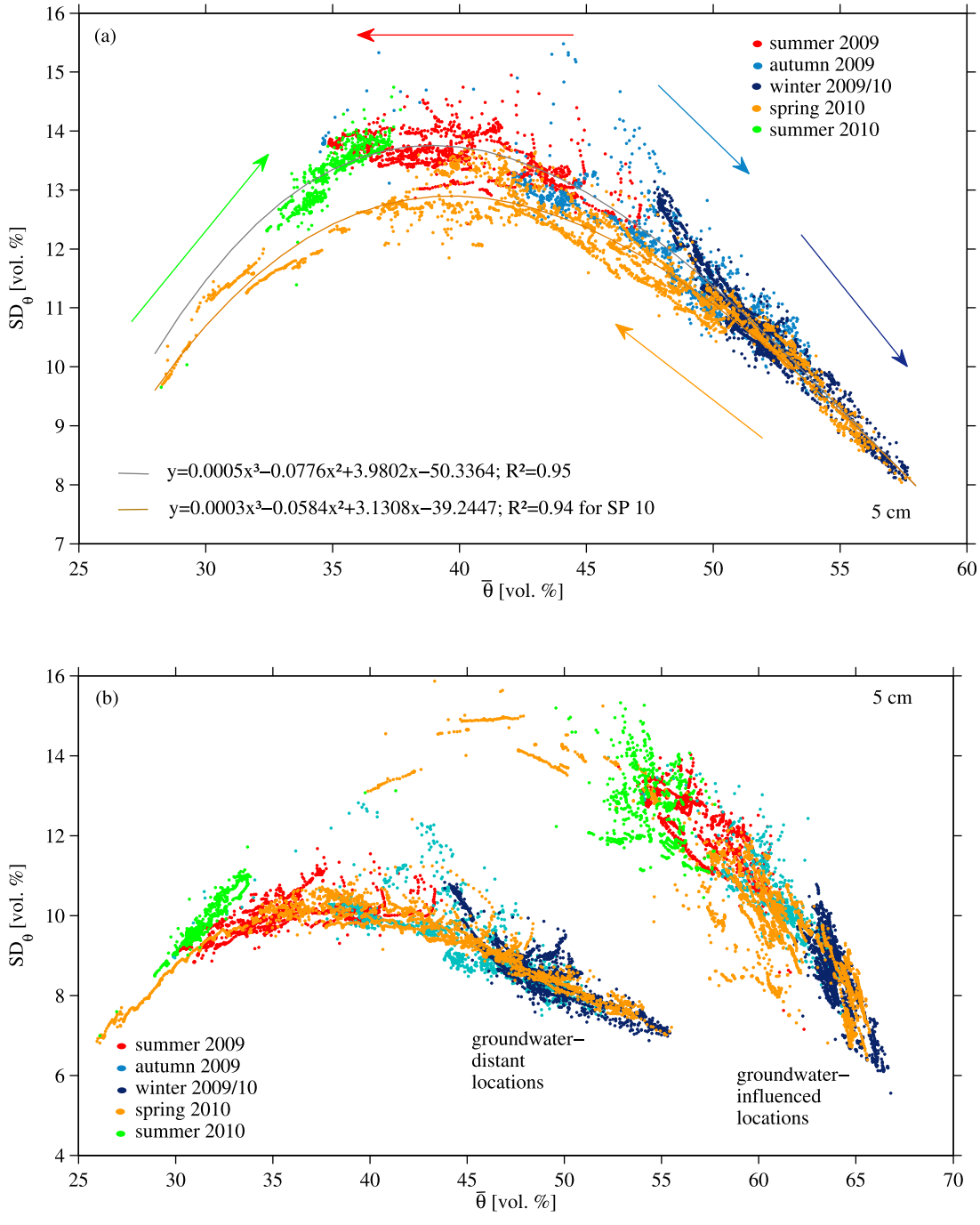

Figure 9. Topsoil $SD_\theta(\overline{\theta})$ for the 1 year data set (a) separated by season and fitted third-order polynomial functions through the spring 2010 data (brown line) and through all other data (gray line); arrows indicate the overall seasonal $SD_\theta(\overline{\theta})$ dynamic. (b) Topsoil $SD_\theta(\overline{\theta})$ for the 1 year data set separated by season and also by measurements in groundwater-distant locations [$SD_{\theta,GWd}(\overline{\theta}_{GWd})$] and groundwater-influenced locations [$SD_{\theta,GWi}(\overline{\theta}_{GWi})$].

in Figure 7 into wetting and drying periods (Figure 11). It is apparent that $SD_\theta(\overline{\theta})$ in the wetting arm was greater than in the drying arm (i.e., hysteresis). This difference is most apparent in the intermediate $\overline{\theta}$ state for the topsoil and seems to be an important source of scatter in the overall topsoil $SD_\theta(\overline{\theta})$ relationship in the intermediate $\overline{\theta}$ range (Figure 7). An elevated SD_θ in the wetting arm as compared with the drying arm was already observed by others for low and intermediate $\overline{\theta}$, e.g., *Vivoni et al.* [2010], and thus seems plausible. At this soil moisture range a set of different interacting wetting and drying controls have to be taken into account (see section 1), whereas SD_θ for high $\overline{\theta}$ is mainly determined by precipitation and the physical limits provided by the soil porosity.

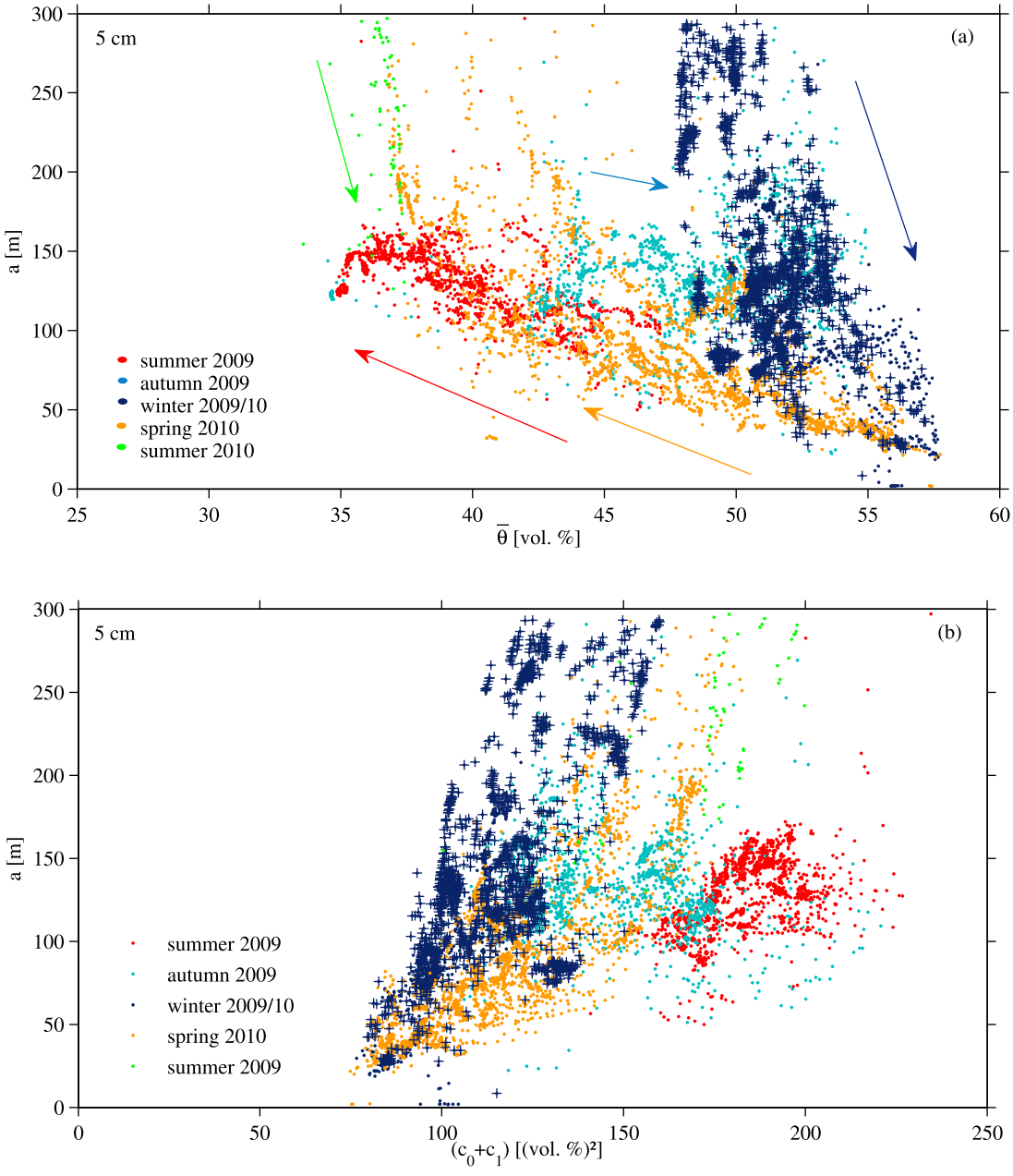

Figure 10. Variogram range as function of (a) mean soil moisture content $[a(\overline{\theta})]$ and (b) total sill $a(c_0 + c_1)$ of the topsoil for the 1 year data set separated by season. Arrows indicate the overall seasonal dynamic and crosses indicate snow accumulation periods in winter 2009/10.

3.7. Spatial Soil Moisture Variability and Autocorrelation for Selected Wetting-Drying Periods at Different Soil Moisture States

[39] To shed light onto the differences in SD_θ for similar $\overline{\theta}$ depending on soil wetting and drying (Figure 11), the temporal dynamics of spatial soil moisture patterns are presented at the event-scale for different soil moisture states (Figures 12–15). For this we selected wetting-drying-periods (WDP) that occurred in the intermediate (WDP2, 5, 8), wet (WDP26), and dry soil moisture state (WDP32) (marked in Figure 3).

3.7.1. Hysteresis in Topsoil $STD(\overline{\theta})$ Dynamics at the Event-Scale–Intermediate Soil Moisture State

[40] The strength of clockwise hysteresis in the topsoil $SD_\theta(\overline{\theta})$ dynamics at the event-scale (Figure 12) varied for different reasons. To highlight this, the hysteresis in $SD_\theta(\overline{\theta})$ dynamics is summarized by means of "characteristic points" ($t1$ to $t6$) that indicate a sign change of $dSD_{\theta/dt}$ or $d\overline{\theta}/dt$ (Figure 12b).

[41] Hysteretic $SD_\theta(\overline{\theta})$ dynamics depended on whether the catchment was wetting or drying. This was analyzed for WDP2 during summer 2009 (Figures 12a and 12b;

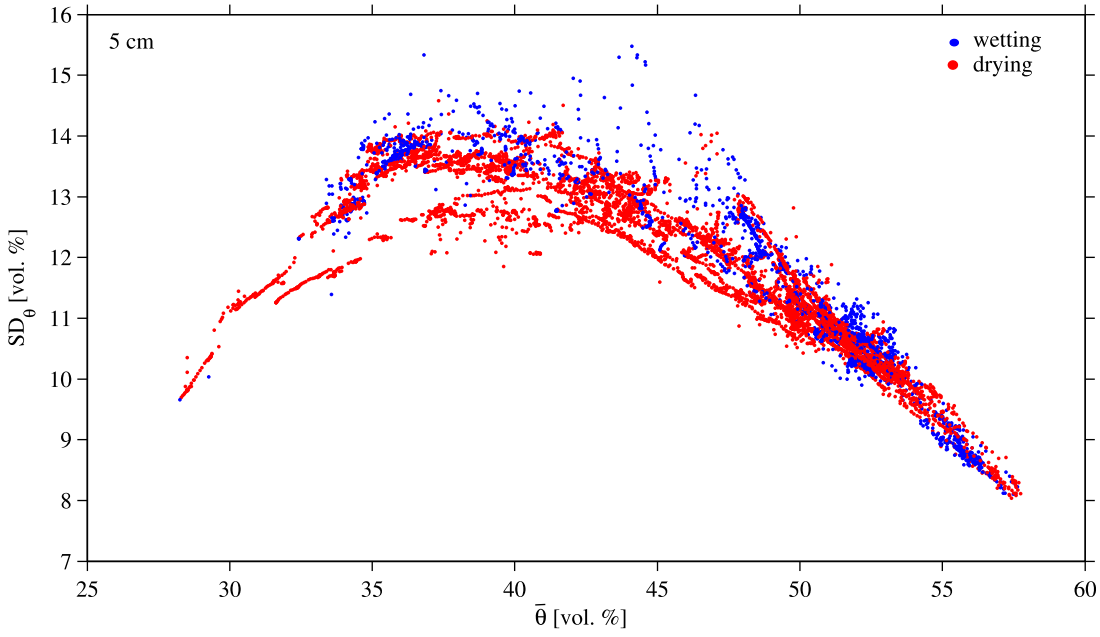

Figure 11. Topsoil SD$_\theta(\overline{\theta})$ of the 1 year data set separated by wetting and drying periods.

Table 2). A rainfall event with a low peak intensity of 4 mm h^{-1} (P_{total} = 17 mm) on intermediate $\overline{\theta}$ ($t1$) rapidly increased topsoil SD$_\theta$ (2 h; $t2$) and $\overline{\theta}$ (19 h; $t3$) in the wetting period. SD$_\theta$ increased during drying ($t4$ to $t5$) and decreased slightly thereafter ($t5$ to $t6$). The spatial soil moisture patterns are characterized by a clear range throughout WDP2 (Figures 13a and 13b; Table 2). The initially intermediate variogram range ($t1$) decreased rapidly early in the wetting period ($t2$) and the spatial soil moisture pattern was reestablished after drying. Groundwater-distant areas showed a larger response during soil wetting and drying than the groundwater-influenced areas.

[42] Distinct hysteresis in topsoil SD$_\theta(\overline{\theta})$ dynamics for intermediate $\overline{\theta}$ was observed for almost all wetting-drying periods in summer 2009 except for WDP5 (Figures 12c and 12d). During this period, a long-lasting low-intensity rainfall event (P_{total} = 24 mm) on moderate $\overline{\theta}$ slowly wet up the topsoil (84 h; $t3$).

[43] Pronounced hysteretic SD$_\theta(\overline{\theta})$ dynamics in the topsoil were also apparent in WDP8 in autumn 2009 (Figures 12e and 12f, Table 2). A long, intense precipitation period (composed of several precipitation events, P_{total} = 67 mm) on moderate $\overline{\theta}$ resulted in a $\overline{\theta}$ increase of about 15 vol. % within one week ($t3$). Early in this period, SD$_\theta$ increased by ~2 vol. % while topsoil $\overline{\theta}$ increased by 10 vol. % within 2 days ($t2$). SD$_\theta$ increased again during drying ($t4$ to $t5$). Again, the variogram range decreased at the beginning of wetting (Table 2, $t2$) but the spatial soil moisture pattern was not reestablished as in WDP2.

[44] In the following, processes driving the topsoil SD$_\theta(\overline{\theta})$ dynamics in the intermediate $\overline{\theta}$ state are discussed. The faster increase in SD$_\theta$ than $\overline{\theta}$ at the beginning of WDP2 is likely to be related to heterogeneous infiltration of low peak intensity precipitation due to heterogeneous interception and throughfall patterns from the spruce canopy [*Jost et al.*, 2004]. Typically, spruce has a high interception storage capacity (2–4 mm), a low amount of stemflow, and concentrated throughfall at the crown periphery [see *Schume et al.*, 2003]. At the onset of precipitation ($t1$), open spaces not covered by spruce wet up faster than areas under spruce due to interception, which leads to a rapid increase in SD$_\theta$ and a decrease of the range at $t2$. The hysteretic effects reported by *Vivoni et al.* [2010] occurred solely during fast soil wetting periods. This supports our observation that hysteretic topsoil SD$_\theta(\overline{\theta})$ dynamics are generated in the intermediate $\overline{\theta}$ state after high intensity precipitation events that rapidly wet the topsoil rather than low intensity long-lasting precipitation that slowly wet the topsoil. In the beginning of WDP2, lateral surface or subsurface flow occurred and resulted in a rapid runoff response. Subsurface $\overline{\theta}$ did not increase during wetting, indicating little vertical water flow. Sometime after passing $t2$, precipitation stopped and SD$_\theta$ started to rapidly decrease for relatively constant $\overline{\theta}$. Soil moisture redistribution and spatially variable, unstressed evapotranspiration were likely the dominant controls for the decrease of SD$_\theta$ during the drying phase, whereas limited water availability for evapotranspiration controlled the increase of SD$_\theta$ later in the WDP. Both, soil moisture redistribution and evapotranspiration were also the main drying controls that reestablished the initial spatial soil moisture pattern.

[45] In addition to hysteresis effects initiated by spatially variable precipitation input, groundwater affected SD$_\theta$ and spatial soil moisture patterns during WDP8. Both groundwater-influenced and groundwater-distant areas showed large responses to precipitation (Figure 13d) leading to increasing SD$_\theta$ and decreasing range ($t2$). The spatial soil moisture patterns were not reestablished after passing $t2$ since the regions influenced by groundwater extended in size at the end of the wetting period, as indicated by a fast increase in groundwater level shown in Figure 4b. Increasing subsoil $\overline{\theta}$ (Figure 3c) indicated relatively fast vertical water flow during wetting. Compared to WDP2, the lower evapotranspiration prevented a rapid drying of the groundwater-distant, upslope areas and an increase in range (Table 2). Thus, the fast

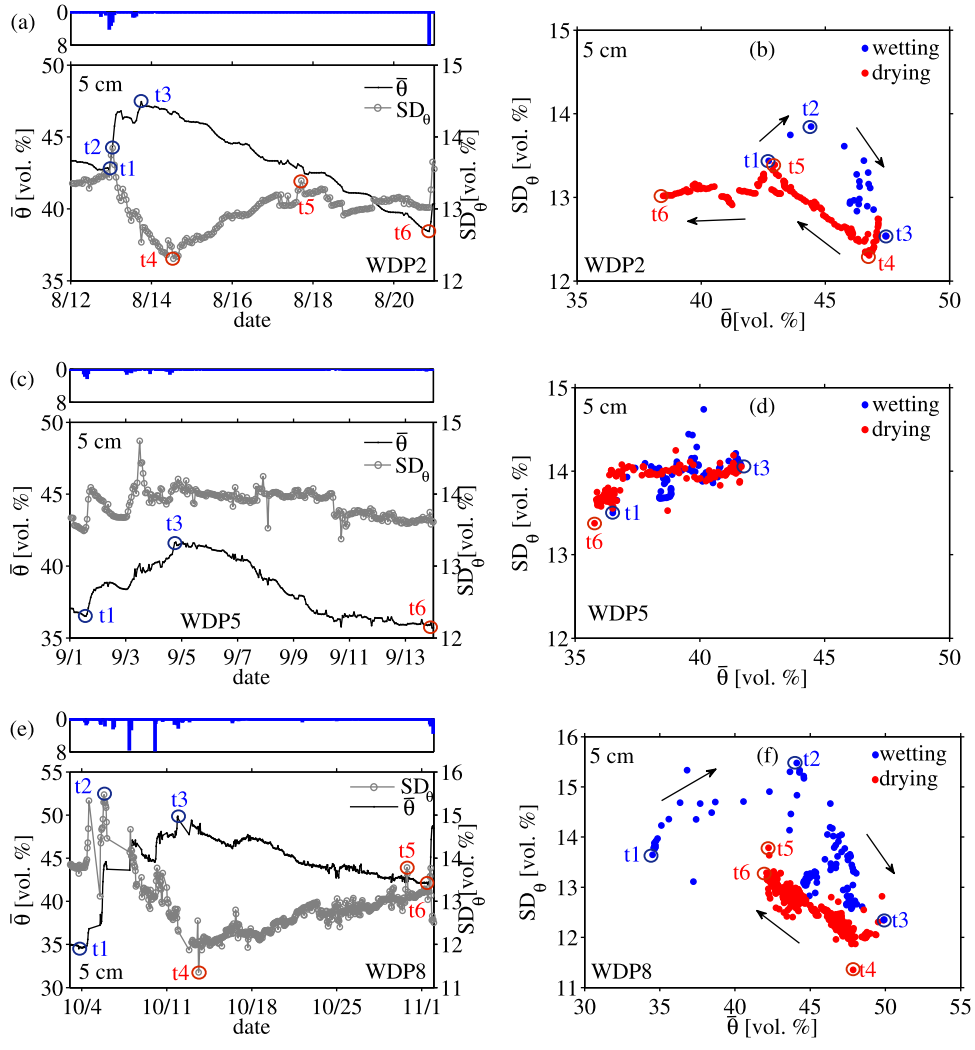

Figure 12. (a, c, e) Time series of precipitation (max. 8 mm h^{-1}): SD_θ (gray line, circles), ($\overline{\theta}$ line, dots); and (b, d, f) $SD_\theta(\overline{\theta})$ at 5 cm depth of the selected event data sets WDP2 (Figures 12a and 12b), WDP5 (Figures 12c and 12d), and WDP8 (Figures 12e and 12f). Characteristic points are provided: {*t*1 [$SD_{\theta,ant}(\overline{\theta}_{ant})$], *t*2 [$SD_{\theta,max}(\overline{\theta}_{crit})_{wet}$], *t*3 [$SD_\theta(\overline{\theta}_{max})$], *t*4 [$SD_{\theta,min}(\overline{\theta})$], *t*5 [$SD_{\theta,max}(\overline{\theta}_{crit})_{dry}$], and *t*6 [$SD_\theta(\overline{\theta}_{min})$]}.

reorganization of spatial structure during the drying observed for WDP2 did not occur for WDP8. Overall, the range of the spatial correlation during WDP2 showed the largest changes, while during WDP8 the total sill showed the largest changes (Figures 13a and 13c).

[46] Summarizing, clockwise hysteretic $SD_\theta(\overline{\theta})$ dynamics at the event-scale are generated in the topsoil for the intermediate $\overline{\theta}$ state after rainfall that rapidly wets up the soil. This was related to intense rainfall and heterogeneous spruce throughfall patterns. $SD_\theta(\overline{\theta})$ hysteresis did not seem to emerge after low-intensity, long-lasting precipitation that slowly wet up the soil. Hysteresis was more pronounced in autumn 2009 when intense precipitation, reduced root water uptake, and increasing groundwater levels contributed to this effect. Finally, the variability in topsoil $SD_\theta(\overline{\theta})$ in the intermediate $\overline{\theta}$ range (Figure 7) was related not only to seasonal $SD_\theta(\overline{\theta})$ dynamics (possibly hysteresis) but also to hysteresis in $SD_\theta(\overline{\theta})$ dynamics at the event-scale (Figures 12b and 12f).

3.7.2. Topsoil Spatial Soil Moisture Patterns—Wet Soil Moisture State

[47] WDP26 (Figures 14a–14d, Table 3) is an example of a wetting and drying event embedded in the drying period during spring 2010. It started in the wet $\overline{\theta}$ state (*x*1). SD_θ and $\overline{\theta}$ were negatively correlated throughout the event (Figure 14a) as expected for the topsoil for the wet state (section 3.3). Initially, intermediate $\overline{\theta}$ was observed in groundwater-distant areas, whereas high $\overline{\theta}$ occurred in groundwater-influenced areas (Figure 14b). In addition, intermediate total sill and variogram range were estimated (Table 3). The range decreased with increasing $\overline{\theta}$ after rainfall (P_{total} = 50 mm). Thereafter, the spatial patterns reestablished during catchment drying (*x*4 to *x*9, Figure 14b) so that drier western, moist eastern upslope areas, and a wetter valley bottom were observed. This was controlled by vertical and lateral flow processes, decreasing groundwater levels (Figure 2b) and also by evapotranspiration when the spruce increased root water uptake. A weak

Table 2. $\overline{\theta}$, SD_θ, Variogram Model Parameters [c_0, $(c_0 + c_1)$, a], the Estimated Nugget Effect [$c_0/(c_0 + c_1)$], and Goodness of Fit (R^2) for the Topsoil for the Characteristic Points $t1$ to $t6$ for the Selected Event Data Set WDP2 and WPD8 (as in Figure 12)

		$\overline{\theta}$	SD_θ	c_0	$(c_0 + c_1)$		$\frac{c_0}{(c_0+c_1)}$	R^2
ti[a]	Date	(vol. %)		(vol. %)^2		a (m)	(–)	
				WDP2 (Summer 2009)				
$t1$	12 Aug 2009 11 pm	42.7	13.4	22.2	185.9	105.2	0.12	0.97
$t2$	13 Aug 2009 1 am	44.4	13.8	27.4	197.9	73.5	0.14	0.88
$t3$	13 Aug 2009 6 pm	47.5	12.5	24.6	175.2	107.7	0.14	0.94
$t4$	14 Aug 2009 1 pm	46.8	12.3	22.7	151.5	107.5	0.15	0.92
$t5$	17 Aug 2009 5 pm	43.0	13.4	19.4	173.0	112.7	0.11	0.96
$t6$	20 Aug 2009 9 pm	38.4	13.0	22.2	180.7	135.6	0.12	0.96
				WDP8 (Autumn 2009)				
$t1$	3 Oct 2009 6 pm	34.5	13.6	11.3	174.5	144.0	0.06	0.96
$t2$	5 Oct 2009 8 pm	44.1	15.5	17.4	215.8	95.9	0.08	0.95
$t3$	11 Oct 2009 10 pm	49.9	12.3	18.5	199.5	108.4	0.09	0.97
$t4$	13 Oct 2009 3 pm	47.9	11.4	10.7	111.8	64.2	0.10	0.89
$t5$	30 Oct 2009 8 pm	42.3	13.6	14.3	190.0	109.4	0.08	0.97
$t6$	1 Nov 2009 12 am	42.0	13.0	17.6	162.6	98.7	0.11	0.98

[a]The characteristic points $t1$ to $t6$ were characterized as follows $t1$ [$SD_{\theta,ant}(\overline{\theta}_{ant})$], $t2$ [$SD_{\theta,max}(\overline{\theta}_{crit})_{wet}$], $t3$ [$SD_\theta(\overline{\theta}_{max})$], $t4$ [$SD_{\theta,min}(\overline{\theta})$], $t5$ [$SD_{\theta,max}(\overline{\theta}_{crit})_{dry}$], and $t6$ [$SD_\theta(\overline{\theta}_{min})$].

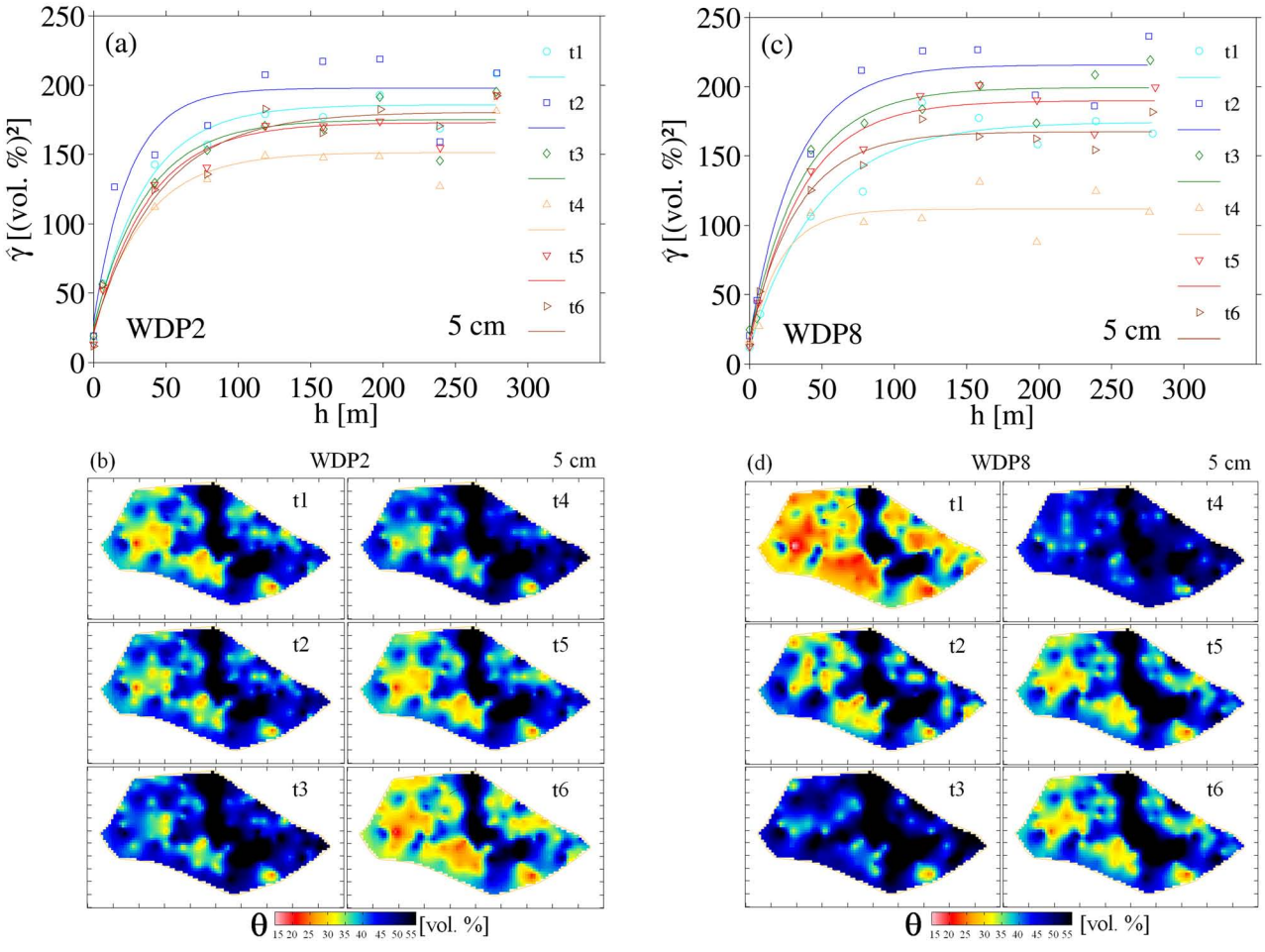

Figure 13. (a, c) Experimental variograms and exponential variogram models and (b, d) kriging maps (using ordinary kriging) for the "characteristic time points" $t1$ to $t6$ at 5 cm depth, respectively. Figures 13a and 13b, event WDP2 (as in Figures 12a and 12b); Figures 13c and 13d, event WDP8 (as in Figures 12e and 12f). Variogram model parameters are provided in Table 2.

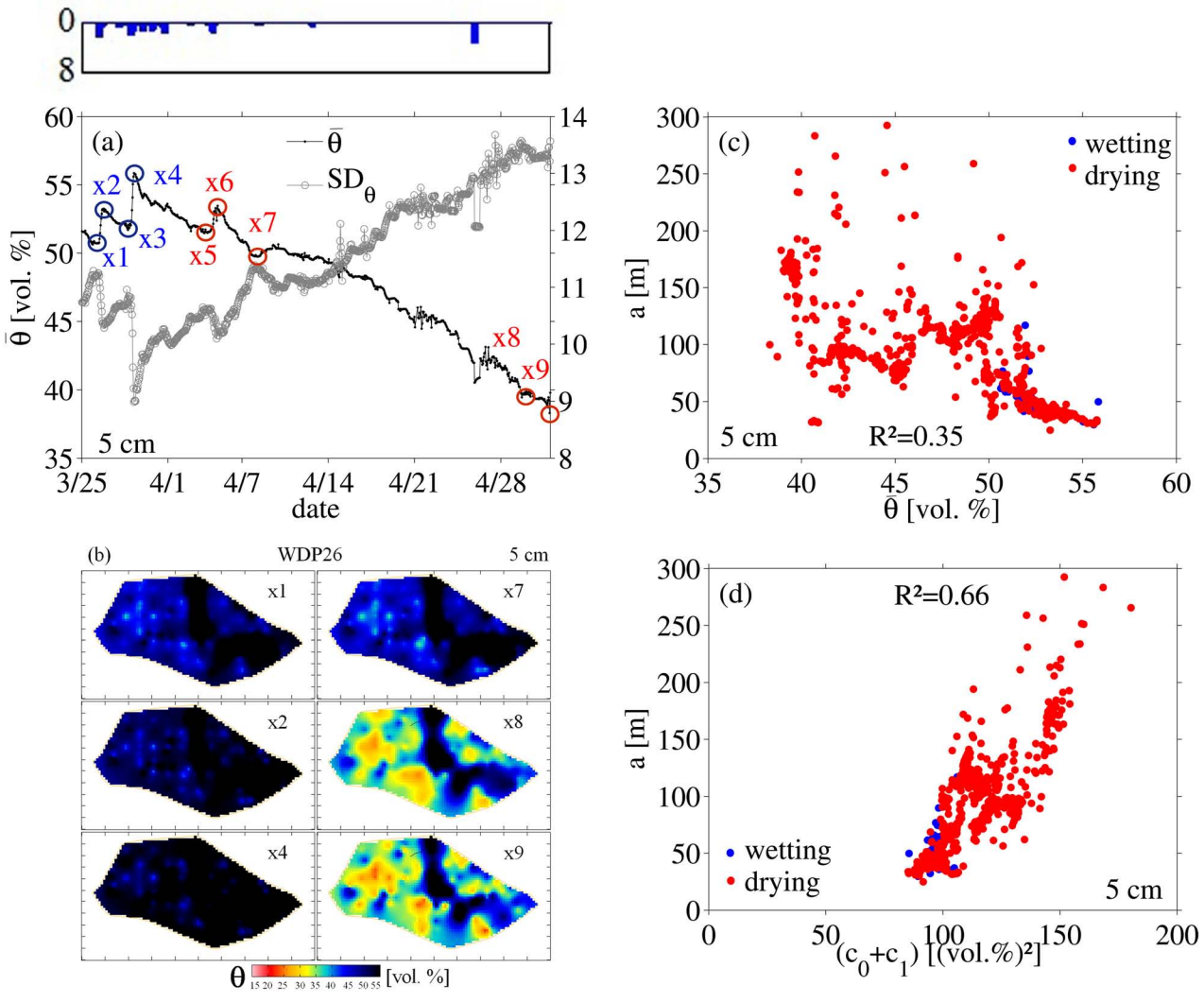

Figure 14. Time series of precipitation (max. 8 mm h^{-1}): (a) $\overline{\theta}$ and SD_θ, (b) kriging maps (ordinary kriging) of selected time stamps x_i, while related variogram model parameters are provided in Table 3; variogram range as function of (c) mean soil moisture content, $a(\overline{\theta})$, (d) variogram range as function of total sill (d) $a[(c_0 + c_1)]$ for WDP26 (spring 2010) at 5 cm depth.

negative relationship between the range and $\overline{\theta}$ was observed, while a moderate positive relationship between the range and total sill was found (Figures 14c and 14d). Thus, in the wet $\overline{\theta}$ state, wetting decreased soil moisture variation and spatial autocorrelation, whereas drying increased soil moisture variation and spatial autocorrelation.

3.7.3. Spatial Soil Moisture Variability—Dry Soil Moisture State

[48] Two intense precipitation events (28 and 12 mm within 1 h) on relatively dry topsoil ($\overline{\theta}$ = 28 vol. %) in summer 2010 resulted in distinct changes in subsoil $\overline{\theta}$ rather than topsoil $\overline{\theta}$ (Figure 15, Table 4) and in rapid runoff-response (hourly runoff of 1.72 mm, Figure 3b). This indicates that a large part of the throughfall quickly bypassed the relatively dry topsoil. This was particularly observed for the initially drier upslope areas where topsoil $\overline{\theta}$ increased by about 4 vol. % only. In contrast, topsoil $\overline{\theta}$ increased by about 13 vol. % in the wetter valley bottom. The observations in the upslope areas are similar to the findings of *Jost et al.* [2004] and *Schume et al.* [2004]. *Jost et al.* [2004] reported that wetting response for low soil moisture in clayey soil under a spruce stand was controlled by preferential flow through a variable macropore system initiated by shrinkage of heavy clayey soil upon drying. This explanation is also plausible for our study site. For example, soil shrinkage was observed during laboratory experiments to determine the permittivity – soil moisture relationship. In addition, it is likely that the high organic carbon content of the forest soil led to hydrophobicity effects. *Schume et al.* [2004] argued that hydrophobicity of spruce litter hindered water infiltration; and repellency has been observed to increase surface runoff in sloping terrain [*Ritsema and Dekker*, 2000]. *Graham and Lin* [2011] found that preferential flow at the upslope areas at the Shale Hills Critical Zone Observatory generally appeared in late summer characterized by low soil moisture and high air temperature. In the lower areas, precipitation and water from the upslope areas (surface and subsurface lateral low) filled the topsoil water storage in the valley bottom. Thus, these areas might have buffered runoff since $\overline{\theta}$ was moderate meaning preferential flow through

Table 3. (Geo-)Statistical Values for the Topsoil for Selected Values x_i of WDP26 (Spring 2010) (see Figure 14)

		$\overline{\theta}$	c_0	$(c_0 + c_1)$		$c_0/(c_0 + c_1)$	R^2
xi[a]	Date	(vol. %)	(vol. %)^2		a (m)	(–)	(–)
			WDP26 (Spring 2010)				
$x1$	25 Mar 2010 10 pm	50.6	25.2	93.5	61.6	0.27	0.84
$x2$	26 Mar 2010 7 pm	53.2	21.1	98.3	37.7	0.22	0.87
$x4$	29 Mar 2010 6 am	55.8	23.9	85.6	49.9	0.28	0.86
$x7$	8 Apr 2010 8 am	49.8	25.7	106.1	73.2	0.24	0.91
$x8$	29 Apr 2010 11 pm	39.8	35.0	158.6	233.9	0.22	0.89
$x9$	1 May 2010 11 pm	38.3	13.6	142.1	99.8	0.10	0.93

[a]Selected time stamps within the spring 2010 event WDP26.

cracks may not have occurred. This is consistent with findings of *Jost et al.* [2004] who found that throughfall recharges topsoil water under comparable precipitation characteristics (quantity and intensity) when $\overline{\theta}$ was moderate. Finally, these different, wetting processes in groundwater-distant and groundwater-influenced areas explain the high gradient of $SD_\theta(\overline{\theta})$ in the beginning of summer 2010 (see section 3.4.) and the distinct occurrence of spatially organized soil moisture patterns in this catchment for some situations. That is, besides the soil moisture, soil texture and precipitation magnitude also contrasts at the larger scale control wetting dynamics of spatial soil moisture patterns.

4. Summary and Conclusions

[49] Our results show that complex, nonlinear soil moisture processes in the Wüstebach catchment are controlled by a variety of interacting factors including soil properties, topography, vegetation, groundwater, meteorological forcing (e.g., rainfall and snow), and the mean soil moisture content. Thus, spatial soil moisture patterns were dependent on depth and soil moisture and changed seasonally and in individual wetting and drying periods.

[50] As expected, spatial soil moisture patterns varied more in the topsoil than at depth. This was due to generally stronger topsoil responses to meteorological forcing and soil water redistribution processes and root water uptake that decreased soil moisture variability and their temporal dynamics at greater depth.

[51] As often reported for the humid climatic zone [e.g., *Western et al.*, 2003], the topsoil $SD_\theta(\overline{\theta})$ relationship of the Wüstebach catchment showed a convex shape which is controlled by deterministic, changing nonlocal (wet soil moisture state) and local factors (dry soil moisture state). Additionally, greater topsoil SD_θ and soil moisture were observed in groundwater-influenced than in groundwater-distant locations indicating significant effects of groundwater. Scatter in topsoil $SD_\theta(\overline{\theta})$ at the intermediate soil moisture state was explained by seasonal and event-scale $SD_\theta(\overline{\theta})$ dynamics.

[52] Seasonal topsoil $SD_\theta(\overline{\theta})$ scatter in the intermediate soil moisture state was most apparent in summer 2009 and

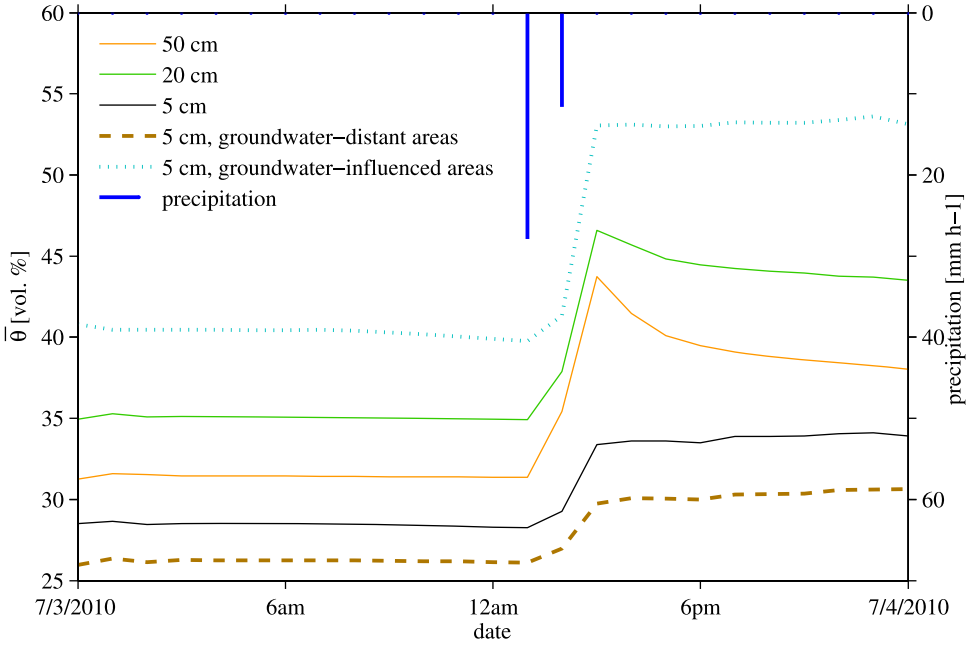

Figure 15. Time series of mean soil moisture ($\overline{\theta}$) on 3 July 2010 at 5, 20, and 50 cm depths as well as topsoil mean soil moisture of groundwater-distant upslope areas (dashed lines, $\overline{\theta}_{GWd}$) and groundwater-influenced areas in the valley bottom (dotted lines, $\overline{\theta}_{GWi}$) of one day in summer 2010.

Table 4. $\overline{\theta}$ and SD_θ for Three Selected Time Stamps on 3 Jul 2010 (in Summer 2010 Event WDP32) at 5, 20, 50 cm Depths and in the Topsoil Separated by Locations With Groundwater Absence and Groundwater Influence

	All Locations						GW Distant[a]		GW Influenced[b]	
	5 cm		20 cm		50 cm		5 cm		5 cm	
Time on 3 Jul 2010	$\overline{\theta}$	SD_θ	$\overline{\theta}$	SD_θ	$\overline{\theta}$	SD_θ	$\overline{\theta}$	SD_θ	$\overline{\theta}$	SD_θ
	(vol. %)									
1 pm	28	10	35	9	31	8	26	7	40	13
2 pm	29	10	38	9	35	8	27	8	41	13
3 pm	33	13	47	10	44	9	30	9	53	14

[a]Groundwater-distant upslope areas.
[b]Groundwater-influenced areas in the valley bottom.

spring 2010. Although the catchment was transitioning from the wet to the dry state in both periods, slightly greater SD_θ was observed for summer 2009. This was because SD_θ remained constantly large in the groundwater-influenced areas in summer 2009. Additionally, large SD_θ was found in the beginning of autumn 2009 and summer 2010 (seasonal wetting transitions) compared with spring 2010 at the same $\overline{\theta}$ due to significant dynamics in soil moisture variability at the event scale controlled by a multitude of factors, particularly groundwater effects. Thus, contrasts at larger spatial scale were important for seasonal $SD_\theta(\overline{\theta})$ dynamics. The behavior described indicates clockwise seasonal $SD_\theta(\overline{\theta})$ hysteresis, but this needs to be confirmed using an analysis of multiple years.

[53] The event-scale topsoil $SD_\theta(\overline{\theta})$ scatter in the intermediate soil moisture range was found to be a result from clockwise hysteretic $SD_\theta(\overline{\theta})$ dynamics that were repeatedly observed and were related to spatially variable throughfall patterns that rapidly increased soil moisture variability. It appeared that hysteretic effects increased with increasing precipitation magnitude, reduced root water uptake, and high groundwater levels. Hysteresis seemed to be absent for low-intensity, uniform precipitation events that slowly wetted up the topsoil.

[54] Our geostatistical analysis led us to the following conclusions: The large-scale variability was larger than the small-scale variability at every depth, despite moderate topsoil nugget-to-total sill-ratio under wet soil moisture conditions (possibly due to errors in soil moisture measurements at high soil moisture content). The range varied significantly over time in the topsoil but not in deeper layers and showed a negative correlation to mean soil moisture content. Spatial soil moisture patterns in the Wüstebach catchment were rough (low variogram range) under very wet soil moisture conditions. Some spatial organization was apparent throughout most of the year, but was stronger in spring and summer 2010 when the upslope areas dried while the valley bottom remained wet due to slowly draining groundwater. Notably, a nonstationary soil moisture distribution was observed after high intensity precipitation on dry soils during summer 2010. This was due to different rewetting behavior in the drier upslope areas (marginal topsoil soil moisture increase possibly due to hydrophobicity and bypassed water related to preferential flow in soil cracks) compared with the moderately wet valley bottom (rainfall and water from the upslope areas refilled the topsoil water storage). Hence, physical factors like topography, groundwater, soil types, vegetation, soil properties, and meteorological forcing caused first-order nonstationarity in the Wüstebach catchment on some occasions. Thus, traditional geostatistical methods were hampered for some situations. Finally, while *Western et al.* [1999] demonstrated seasonal variation between both random and organized soil moisture fields in the Tarrawarra test site, our study extended this to event-scale development of random to organized soil moisture fields.

[55] This research showed that soil properties, topography, vegetation, groundwater and mean soil moisture content were key factors in explaining the drying arm. It also showed that in addition to these key factors the characteristics of meteorological forcing, particularly rainfall intensity, influenced the evolution of spatial soil moisture patterns during wetting periods. This study also highlighted that hourly monitoring of the profile across the catchment was crucial to detect abrupt transitions, generated predominantly during soil rewetting, and to inform long-term dynamics of spatial soil moisture patterns. Our work demonstrated the ability of a wireless sensor network to routinely monitor soil moisture with high temporal and spatial resolution and coverage. The resulted unique data set describing the event scale and seasonal dynamics of spatial soil moisture patterns at the catchment scale can be used to test assumptions and ideas on underlying controls and processes and to verify the ability of hydrologic models to capture spatial soil moisture variability. Further on, geostatistical analyses of the soil moisture patterns enable the optimization of the spatial sampling design [*Bogena et al.*, 2010] as well as in-depth comparison of the spatial auto-correlation in simulation results with the experimentally derived spatial autocorrelation [*Herbst and Diekkrüger*, 2003] over time.

Appendix A: Obtaining Soil Moisture Data

[56] Soil moisture was determined from sensor response using a two-step-approach [see also *Jones et al.*, 2005]. First, the sensor response v was related to the apparent dielectric sensor permittivity (K_a, –) using an empirical sensor response-permittivity (SRP) model for each sensor type. As proposed by *Rosenbaum et al.* [2010], we used the following for the EC-5 sensor:

$$\sqrt{K_a} = 0.0001v^{1.6784} + 0.0807 \quad \text{(A1)}$$

and for the 5TE sensor:

$$K_a = 0.0234v - 1.2917. \quad \text{(A2)}$$

[57] These relationships were derived from sensor response measurements of 105 EC-5 and 105 5TE sensors in dielectric liquids with known permittivities ranging from 2 to 35. The root mean square error (RMSE) between predicted and reference permittivity was 1.5 for the EC-5 sensor and 1.2 for the 5TE sensor.

[58] In the second step, the apparent dielectric permittivity was converted to soil moisture. To obtain this relationship for the Wüstebach test site, in total 14 undisturbed samples (length = 7.7 cm, diameter = 5 cm) were taken from two different depths, ranging from approximately 5 to 13 cm and 20 to 28 cm, for the main soil types (Cambisols, Planosols, Gleysols). The mean and the standard deviation (SD) of the soil texture, organic carbon, and bulk density of these 14 samples are provided in Table A1. First, the samples were saturated. The mean saturated soil moisture was 61 vol. % with a standard deviation of 8 vol. %. Next, the samples were dried at room temperature and the volumetric soil moisture and dielectric permittivity were determined at regular time intervals. The volumetric soil moisture was determined from the weight of the sample, the known sample volume, and the dry weight of the sample determined at the end of the experiment by oven drying (65°C, 48 h). Artificial decreases in volume due to shrinkage occurred in eight samples and were corrected by considering the volume decrease. The apparent dielectric permittivity of each sample was determined from measurements with a CS 640-L 3-rod TDR probe attached to a TDR 100 device (Campbell Scientific, Logan, UT). A custom MatLab algorithm based on the travel time analysis algorithm presented by *Heimovaara and Bouten* [1990] was used to analyze the TDR measurements.

[59] Five soil samples had to be discarded either because shrinkage caused air gaps between the TDR probe head and soil or because the samples turned out to contain a large volume of roots or stones, which was deemed to be unrepresentative of the sampling locations. Therefore, the final data set describing the relationship between dielectric permittivity and soil moisture consisted of nine soil samples (Figure A1). Since the data density was not equal over the soil moisture range, the data were binned into nine permittivity classes (from 0 to 45 with a bin size of 5) and the average dielectric permittivity and soil moisture were calculated for each bin. Six empirical and semitheoretical models were fitted to the binned data and the performance of each of these six models was judged using the RMSE for the entire data set shown in Figure A1. It was found that several models performed equally well (results not shown). One of the models that performed well was the complex refractive index model (CRIM) proposed by *Birchak et al.* [1974], which used parameter values from the literature rather than fitting (Figure A1):

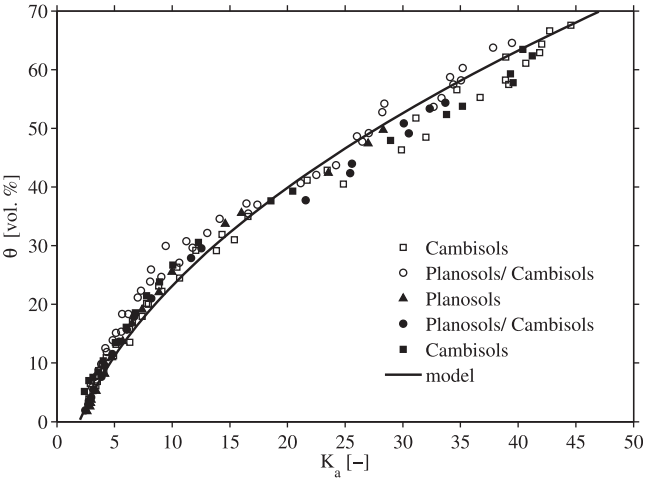

Figure A1. Apparent dielectric sensor permittivity (K_a)–soil moisture (θ) data for a few soil samples of the topsoil (sampling in ~5–13 cm depth; open symbols) and subsurface soil (sampling in ~20–28 cm depth; filled symbols) of the TERENO test site Wüstebach and the derived apparent dielectric permittivity–soil moisture model (equation (A3)).

$$\theta = 100 * \frac{K_a^{\beta} - (1-\eta)\cdot K_s^{\beta} - \eta K_{\text{air}}^{\beta}}{K_w(T)^{\beta} - K_{\text{air}}^{\beta}}, \quad \text{(A3)}$$

where K_a is the measured apparent dielectric sensor permittivity, the shape factor β is assumed to be 0.5 [*Pepin et al.*, 1995], the dielectric permittivity of the solid phase K_s is assumed to be 4.4 [*Robinson et al.*, 2004], the dielectric permittivity of air K_{air} is 1, the mean porosity η is estimated to be 0.624, and the temperature dependent dielectric permittivity of water for 25°C (room temperature in the laboratory) is 78.54 according to *Weast et al.* [1986] and θ is given in vol. %. The RMSE of equation (A3) was 2.9 vol. %.

[60] Because of the relatively high accuracy of equation (A3), it was deemed sufficient to use a single site-specific calibration relationship. The consideration of bulk density and other soil properties did not strongly improve the accuracy of the calibration relationship. The small increase in accuracy that potentially can be achieved with a more elaborate calibration relationship did not weigh up against the additional effort to obtain accurate data on the spatial variability of the additional soil properties used in such a calibration relationship.

[61] The effects of temperature on soil moisture measurements with dielectric sensors is known to be complicated [e.g., *Wraith and Or*, 1999; *Or and Wraith*, 1999]. It is

Table A1. Major Properties of the Samples for the Topsoil and Subsurface Soil That Were Used in the Experiment for Derivation of the Permittivity-Soil Moisture Relationship

	~5–13 cm		~20–28 cm	
Sample Property	Mean	SD	Mean	SD
Sand (%)	8.2	3.1	9.5	3.8
Silt (%)	62.1	4.1	59.4	5.5
Clay (%)	29.7	4.1	31.2	6.9
Corg. (%)	11.7	3.5	5.0	2.3
Bulk Density (g cm^{-3})	0.89	0.14	1.16	0.25

important to separate between the effect of temperature on the dielectric measurement and the effect of temperature on the dielectric properties of the soil. Previous laboratory experiments have shown that temperature affects K_a measurements using the EC-5 and the 5TE sensor [*Bogena et al.*, 2007; *Rosenbaum et al.*, 2011] which can be corrected for temperatures between 5 and 40°C [*Rosenbaum et al.*, 2011]. However, the temperature sensitivity of the soil dielectric properties has not been investigated in detail for the soils in the Wüstebach area. It was shown in *Rosenbaum et al.* [2011] that application of the temperature correction to the sensor measurements introduces a stronger temperature dependence of K_a (Figure 4 of that study). For soils without high surface area clays, a subsequent correction of the measured K_a to 25°C almost completely removed the temperature correction again, indicating that the temperature effect on the sensor response and the soil dielectric properties cancel each other. Therefore, we decided not to apply a correction for temperature. This is better than just correcting for the sensor temperature effect on the sensor, as this would introduce considerable temperature sensitivity that cannot currently be removed due to the lack of an appropriate model for the temperature sensitivity of the Wüstebach soil dielectric properties.

[62] K_a measurements from the EC-5 and the 5TE sensor are also affected by bulk electrical conductivity [*Bogena et al.*, 2007; *Rosenbaum et al.*, 2011]. The mean bulk electrical conductivity was constantly quite low in our study period (data not shown). It ranged from 0.02 to 0.1 dS m^{-1} with an average of 0.04 dS m^{-1} at the 5 cm depth and it was lower at 50 cm. Higher bulk electrical conductivity was observed at locations influenced by groundwater (soil types 3–5; mean of 0.06 dS m^{-1} at 50 cm depth). *Rosenbaum et al.* [2011] showed that the effect of electrical conductivity on K_a is small in this electrical conductivity range. Furthermore, they recommended not applying the conductivity correction function for very low bulk electrical conductivity in order to avoid unnecessary corrections that would only introduce uncertainties [*Rosenbaum et al.*, 2011]. Therefore, K_a measurements were not corrected for effects of bulk electrical conductivity.

[63] **Acknowledgments.** We gratefully acknowledge the support by the SFB-TR32 "Pattern in Soil-Vegetation-Atmosphere Systems: Monitoring, Modeling and Data Assimilation" funded by the Deutsche Forschungsgemeinschaft (DFG) and TERENO (Terrestrial Environmental Observatories) funded by the Helmholtz-Gemeinschaft. We thank Meteomedia for providing meteorological data. We furthermore thank Ferdinand Engels, Rainer Harms, Nirca Gerl, and Michael Schraven for support during deployment of the network and Bernd Schilling for ongoing maintenance. The data used in this study are already freely available via the TERENO data portal TEODOOR (http://teodoor.icg.kfa-juelich.de/). Downloading all sensor network data for a long period of time is problematic because of the large amount of data. Therefore, the entire data set is also available from the authors upon request.

References

Beier, C., K. Hansen, and P. Gundersen (1993), Spatial variability of throughfall fluxes in a spruce forest, *Environ. Pollut.*, *81*, 257–267, doi:10.1016/0269-7491(93)90208-6.

Birchak, J. R., C. G. Gardner, J. E. Hipp, and J. M. Victor (1974), High dielectric constant microwave probes for sensing soil moisture, *Proc. IEEE*, *62*(1), 93–98, doi:10.1109/proc.1974.9388.

Blonquist, J. M., S. B. Jones, and D. A. Robinson (2005), Standardizing characterization of electromagnetic water content sensors: 2. Evaluation of seven sensing systems, *Vadose Zone J. 4*, 1059–1069. doi:10.2136/vzj2004.0141.

Blume, T., E. Zehe, and A. Bronstert (2009), Use of soil moisture dynamics and patterns at different spatio-temporal scales for investigation of subsurface flow processes, *Hydrol. Earth Syst. Sci.*, *13*, 1215–1234, doi:10.5194/hessd-4-2587-2007.

Bogena, H. R., J. A. Huisman, C. Oberdörster, and H. Vereecken (2007), Evaluation of a low-cost soil water content sensor for wireless network applications, *J. Hydrol.*, *344*, 32–42, doi:10.1016/j.jhydrol.2007.06.03.

Bogena, H. R., J. A. Huisman, H. Meier, U. Rosenbaum, and A. Weuthen (2009), Hybrid wireless underground sensor networks. Quantification of signal attenuation in soil, *Vadose Zone J.*, *8*(3), 755–761, doi:10.2136/vzj2008.0138.

Bogena, H. R., M. Herbst, J. A. Huisman, U. Rosenbaum, A. Weuthen, and H. Vereecken (2010), Potential of wireless sensor networks for measuring soil water content variability, *Vadose Zone J.*, *9*(4), 1002–1013, doi:10.2136/vzj2009.0173.

Bouten, W., T. J. Heimovaara, and A. Tiktak (1992), Spatial patterns of throughfall and soil water dynamics in a Douglas fir stand, *Water Resour. Res.*, *28*(12), 3227–3233, doi:10.1029/92WR01764.

Chen, D., C.-T. Lu, Y. Kou, and F. Chen (2008), On detecting spatial outliers, *Geoinformatica*, *12*, 455–475, doi:10.1007/s10707-007-0038-8.

Choi, M., and J. M. Jacobs (2007), Soil moisture variability of root zone profiles within SMEX02 remote sensing footprints, *Adv. Water Resour.*, *30*, 883–896, doi:10.1016/j.advwatres.2006.07.007.

Cobos (2008), EC-5 Volume of Sensitivity, Decagon Appl. Note 13931-00 AN, [Available at, http://www.decagon.com/assets/Uploads/EC-5-Volume-of-Sensitivity.pdf, verified 9 Oct. 2012.] Decagon Devices, Inc., Pullman, Wash.

De Lannoy, G. J. M., N. E. C. Verhoest, P. R. Houser, T. J. Gish, and M. V. Meirvenne (2006), Spatial and temporal characteristics of soil moisture in an intensively monitored agricultural field (OPE^3), *J. Hydrol.*, *331*, 719–730, doi:10.1016/j.jhydrol.2006.06.016.

Deutsch, C. V., and A. G. Journel (1998), *GSLIB, Geostatistical software library and user's guide*, 2nd ed., Oxford Univ. Press, New York.

Etmann, M. (2009), *Dendrologische Aufnahmen im Wassereinzugsgebiet Oberer Wüstebach anhand verschiedener Mess- und Schätzverfahren*, Diplomarbeit, Münster, Germany.

Famiglietti, J. S., J. W. Rudnicki, and M. Rodell (1998), Variability in surface moisture content along a hillslope transect: Rattlesnake Hill, Texas, *J. Hydrol.*, *210*(1–4), 259–281, doi:10.1016/S0022-1694(98)00187-5.

Fernandez-Illescas, C. P., A. Porporato, F. Laio, and I. Rodriguez-Iturbe (2001), The ecohydrological role of soil texture in a water-limited ecosystem, *Water Resour. Res. 37*(12), 2863–2872.

Graham, C. B., and H. Lin (2011), Controls and frequency of preferential flow occurrence. A 175-event analysis, *Vadose Zone J.*, *10*(3), 816–831, doi:10.2136/vzj2010.0119.

Grayson, R. B., and G. Blöschl (Eds.) (2000), *Spatial Patterns in Catchment Hydrology. Observations and Modelling*, 406 pp., Cambridge Univ. Press, Cambridge.

Grayson, R. B., A. W. Western, F. Chiew, and G. Blöschl (1997), Preferred states in spatial soil moisture patterns: Local and nonlocal controls, *Water Resour. Res.*, *33*(12), 2897–2908, doi:10.1029/97WR02174.

Heimovaara, T. J., and W. Bouten (1990), A computer-controlled 36-channel time domain reflectometry system for monitoring soil water contents, *Water Resour. Res.*, *26*, 2311–2316, doi:10.1029/WR026i010p02311.

Herbst, M. and B. Diekkrüger (2003), Modelling the spatial variability of soil moisture in a micro-scale catchment and comparison with field data using geostatistics, *Phys. Chem. Earth. 28*, 239–245, http://dx.doi.org/10.1016/S1474-7065(03)00033-0.

Hupet, F., and M. Vanclooster (2002), Intraseasonal dynamics of soil moisture variability within a small agricultural cropped field, *J. Hydrol.*, *261*, 86–101, doi:10.1016/S0022-1694(02)00016-1.

Ivanov, V. Y., S. Fatichi, G. D. Jenerette, J. F. Espeleta, P. A. Troch, and T. E. Huxman (2010), Hysteresis of soil moisture spatial heterogeneity and the "homogenizing" effect of vegetation, *Water Resour. Res.*, *41*, W09521, doi:10.1029/2009WR008611.

Jones, S. B., J. M. Blonquist, D. A. Robinson, V. Philip Rasmussen, and D. Or (2005), Standardizing characterization of electromagnetic water content sensors, Part 1. Methodology, *Vadose Zone J.*, *4*, 1048–1058, doi:10.2136/vzj2004.0140.

Jost, G., H. Schume, and H. Hager (2004), Factors controlling soil water-recharge in a mixed European beech (Fagus sylvatica L.)-Norway spruce

[Picea abies (L.) Karst.] stand, *Eur. J. Forest Res.*, *123*, 93–104, doi:10.1007/s10342-004-0033-7.

Jost, G., G. B. M. Heuvelink, and A. Papritz (2005), Analysing the space-time distribution of soil water storage of a forest ecosystem using spatio-temporal kriging, *Geoderma*, *128*, 258–273, doi:10.1016/j.geoderma.2005.04.008.

Kou, Y. (2006), Spatial weighted outlier detection, in *Abnormal Pattern Recognition in Spatial Data*, PhD Diss., Virginia Polytechnic Inst. and State Univ., Falls Church.

Lawrence, J. E., and G. M. Hornberger (2007), Soil moisture variability across climate zones, *Geophys. Res. Lett.*, *34*, L20402, doi:10.1029/2007GL031382.

Lin, H. (2006), Temporal stability of soil moisture spatial pattern and subsurface preferential flow pathways in the Shale Hills Catchment, *Vadose Zone J.*, *5*, 317–340, doi:10.2136/vzj2005.0058.

Nash, J. E., and J. V. Sutcliffe (1970), River flow forecasting through conceptual models part I—A discussion of principles, *J. Hydrol.*, *10*(3), 282–290, doi:10.1016/0022-1694(70)90255-6.

Nyberg, L. (1996), Spatial variability of soil water content in the covered catchment at Gårdsjön, Sweden, *Hydrol. Processes*, *10*, 89–103, doi:10.1002/(SICI)1099-1085(199601).

Or, D., and J. M. Wraith (1999), Temperature effects on soil bulk dielectric permittivity measured by time domain reflectometry: A physical model, *Water Resour. Res. 35*, 371–383, doi:10.1029/1998WR900008.

Pan, F., and C. D. Peters-Lidard (2008), On the relationship between mean and variance of soil moisture fields, *J. Am. Water Resourc. Assoc.*, *41*(1), 235–242, doi:10.1111/j.1752-1688.2007.00150.x.

Pepin, S., N. J. Livingston, and W. R. Hook (1995), Temperature dependent measurement errors in time domain reflectometry determination of soil water, *Soil Sci. Soc. Am. J.*, *59*, 38–43, doi:10.2136/sssaj1995.03615995005900010006x.

Richter, F. (2008), Bodenkarte zur Standorterkundung. Verfahren Quellgebiet Wüstebachtal (Forst). (Forst), Geol. Dienst Nordrhein-Westfalen, Krefeld, Germany.

Ritsema C. J., and L. W. Dekker (2000), Preferential flow in water repellent sandy soils. Principles and modelling implications, *J. Hydrol.*, *231-232*, 308–319, doi:10.10.16/S0022-1694(00)00203-1.

Robinson, D. A. (2004), Measurement of the solid dielectric permittivity of clay minerals and granular samples using a time domain reflectometry immersion method, *Vadose Zone J.*, *3*(2), 705–713, doi:10.2136/vzj2004.0705.

Robinson, D. A., C. S. Campbell, J. W. Hopmans, B. K. Hornbuckle, S. B. Jones, R. Knight, F. Ogden, J. Selker, and O. Wendroth (2008), Soil moisture measurement for ecological and hydrological watershed-scale observatories. A review, *Vadose Zone J.*, *7*, 358–389, doi:10.2136/vzj2007.0143.

Rosenbaum, U., J. A. Huisman, A. Weuthen, H. Vereecken, and H. R. Bogena (2010), Sensor-to-sensor variability of the ECH2O EC-5, TE, and 5TE sensors in dielectric liquids, *Vadose Zone J.*, *9*, 181–186, doi:10.2136/vzj2009.0036.

Rosenbaum, U., J. A. Huisman, J. Vrba, H. Vereecken, and H. R. Bogena (2011), Correction of temperature and electrical conductivity effects on dielectric permittivity measurements with ECH2O sensors, *Vadose Zone J.*, *10*, 582–593, doi:10.2136/vzj2010.0083.

Ryu, D., and J. S. Famiglietti (2005), Characterization of footprint-scale surface soil moisture variability using Gaussian and beta distribution functions during the Southern Great Plains 1997 (SGP97) hydrology experiment, *Water Resour. Res.*, *41*, W12433, doi:10.1029/2004WR003835.

Schume, H., G. Jost, and K. Katzensteiner (2003), Spatio-temporal analysis of the soil water content in a mixed Norway spruce (*Picea abies* (L.)) – European beech (*Fagus sylvatica* L.) stand, *Geoderma*, *112*, 273–287, doi:10.1016/S0016-7061(02)00311-7.

Schume, H., G. Jost, and H. Hager (2004), Soil water depletion and recharge patterns in mixed and pure forest stands of European beech and Norway spruce, *J. Hydrol.*, *289*, 258–274, doi:10.1016/j.jhydrol.2003.11.036.

SoilNet (2011), [Now at http://www.fz-juelich.de/ibg/ibg-3/EN/About/%20us/Tereno/SoilNet/SoilNet.html, verified 25 Sept. 2012.]

Takagi, K., and H. S. Lin (2011), Temporal Dynamics of soil moisture spatial variability in the Shale Hills Critical Zone Observatory, *Vadose Zone J.*, *10*, 3, 832–842, doi:10.2136/vzj2010.0134.

TERENO (2011), Forschungszentrum Jülich, Jülich, Germany. [Available at http://teodoor.icg.kfa-juelich.de/, verified 9 Oct. 2012.]

Teuling, A. J., and P. A. Troch (2005), Improved understanding of soil moisture variability dynamics, *Geophys. Res. Lett.*, *32*, L05404, doi:10.1029/2004GL021935.

Teuling, A. J., F. Hupet, R. Uilenhoet, and P. Troch (2007), Climate variability effects on spatial soil moisture dynamics, *Geophys. Res. Lett.*, *34*, L06406, doi:10.1029/2006GL029080.

Vereecken, H., T. Kamai, T. Harter, R. Kasteel, J. Hopmans, and J. Vanderborght (2007), Explaining soil moisture variability as a function of mean soil moisture, A stochastic unsaturated flow perspective, *Geophys. Res. Lett.*, *34*, L22402, doi:10.1029/2007GL031813.

Vereecken, H., J. A. Huisman, H. R. Bogena, J. Vanderborght, J. A. Vrugt, and J. W. Hopmans (2008), On the value of soil moisture measurements in vadose zone hydrology. A review, *Water Resour. Res.*, *44*, W00D06, doi:10.1029/2008WR006829.

Vivoni, E. R., J. C. Rodríguez, and C. J. Watts (2010), On the spatiotemporal variability of soil moisture and evapotranspiration in a mountainous basin within the North American monsoon region, *Water Resour. Res.*, *46*, W02509, doi:10.1029/2009WR008240.

Walker, J., G. Willgoose, and J. Kalma (2004), In situ measurement of soil moisture: A comparison of techniques, *J. Hydrol.*, *293*(1–4), 85–99, doi:10.1016/j.jhydrol.2004.01.008.

Weast, R. C. (Ed.) (1986), *Handbook of Physics and Chemistry*, 67th ed., CRC, Boca Raton, FL.

Western, A. W., and G. Blöschl (1999), On spatial scaling of soil moisture, *J. Hydrol.*, *217*, 203–224, doi:10.1016/S0022-1694(98)00232-7.

Western, A. W., and R. B. Grayson (1998), The Tarrawarra data set: Soil moisture patterns, soil characteristics, and hydrological flux measurements, *Water Resour. Res.*, *34*(10), 2765–2768. doi:10.1029/98WR01833.

Western, A. W., G. Blöschl, and R. B. Grayson (1998), Geostatistical characterization of soil moisture patterns in the Tarrawarra catchment, *J. Hydrol.*, *205*, 20–37, doi:10.1016/S0022-1694(97)00142-X.

Western, A. W., R. B. Grayson, G. Blöschl, G. R. Willgoose, and T. A. McMohan (1999), Observed spatial organization of soil moisture and its relation to terrain indices, *Water Resour. Res.*, *35*(3), 797–810, doi:10.1029/1998WR900065.

Western, A. W., R. B. Grayson, and G. Blöschl (2002), Scaling of soil moisture. *A hydrologic perspective, Annu. Rev. Earth Planet. Sci.*, *30*, 149–180, doi:10.1146/annurev.earth.30.091201.140434.

Western, A. W., R. B. Grayson, G. Blöchl, and D. J. Wilson (2003), Spatial variability of soil moisture and its implications for scaling, in *Scaling Methods in Soil Physics*, edited by Y. Pachepsky, D. E. Radcliff, and H. M. E. Selim, CRC, Boca Raton, FL.

Wraith, J. M., and D. Or (1999), Temperature effects on soil bulk dielectric permittivity measured by time domain reflectometry: Experimental evidence and hypothesis development, *Water Resour. Res. 35*, 361–369, doi:10.1029/1998WR900006.

Zacharias, S., et al. (2011), A network of terrestrial environmental observatories in Germany, *Vadose Zone J.*, *10*, 955–973, doi:10.2136/vzj2010.0139.

Zehe, E., T. Graeff, M. Morgner, A. Bauer, and A. Bronstert (2010), Plot and field scale soil moisture dynamics and subsurface wetness control on runoff generation in a headwater in the Ore Mountains, *Hydrol. Earth Syst. Sci.*, *14*, 873–889, doi:10.5194/hess-14-873-2010.